Bulletin of the Earthquake
Research Institute
University of Tokyo
Vol. 62 (1987) pp. 163-200

Scattering of Rayleigh Waves by a Semi-circular Rough Surface on Layered Media

Takao Momoi
Earthquake Research Institute, the University of Tokyo, Japan

(Received July 30, 1987)

Abstract

The expressions for the energy of the scattered waves are theoretically obtained for the incidence of a train of periodic Rayleigh waves upon the semi-circular mountain in the semi-infinite elastic space with the upper layer. The evaluation of these expressions was carried out numerically.

In the model with the upper layer we can expect two types of trapped waves along the free surface and the interface. One is the well-known Rayleigh waves which exponentially decrease in amplitude toward the inside of the medium. The other is the waves which have trigonometric components in the inside of the lower medium. The second type of waves is named as *leaky mode*.

The waves of leaky mode, though very unstable, have strong effects on the partition of the energy in the scattering problem considered here. In the problems of the surface waves along the plane free surface the study of the leaky mode of the waves has been omitted so far, because it readily disappears due to the unstableness of the waves. However, in the problems along the irregular surface the importance of this type of waves arise.

In general, occurrences of the resonant standing P and S waves of leaky mode cause the depression of the transmissibility of the energy of the transmitted waves and, as a reciprocal effect, cause an increase of the energy of the scattered body waves, particularly the S waves.

Even in the model with the upper layer (this study) we can expect the same behavior of the energy of the transmitted Rayleigh waves as that in the case without the upper layer (studied before). That is to say, (a) the occurrences of the resonant standing S and P waves in the mountain results in an abrupt decrease of the transmissibility of the transmitted Rayleigh waves through the mountain, and (b) on the contary, the standing Rayleigh waves along the curved surface causes the inverse result, i.e., the higher transmissibility of the transmitted Rayleigh waves.

1. Introduction

Rigorous analytical solutions to propagation problems involving elastic surface waves are known only for a limited number of geometrical configurations, including homogeneous half spaces (LAMB, 1904) and simple layered media (EWING *et al.*, 1957). Problems involving geometries, such as the homogeneous and inhomogeneous quarter planes, and some kinds of rough surfaces, have proved to be analytically intractable.

The propagation of elastic waves in media presenting rough surfaces has received much attention. Lots of studies on this problem were carried out and are reviewed in WOODHOUSE (1974). In some papers (SUTEAU and MARTEL, 1980; DOORNBOS, 1978; CISTERNAS and JOBERT, 1977), a perturbation method is used so that only localized, slight irregularities are studied.

With the development of high-speed computers, wave problems due to irregular rough surface have been studied by use of the method of finite difference (SATÔ, 1972; MARTEL *et al.*, 1977; FUYUKI and MATSUMOTO, 1980) or finite element (LYSMER and DRAKE, 1971, 1972; DRAKE, 1972; ZAMA, 1981).

In the case of a trench in the half elastic space, Rayleigh waves scattered there have been studied experimentally (FUJII *et al.*, 1980 a, b, and c), and then the other related studies are shortly reviewed in their works. These studies have brought out various interesting characteristics of the transmitted Rayleigh waves.

As a result various results have been obtained, but there still exist many unresolved problems.

Succeeding previous studies on the scattering of Rayleigh waves by a semi-circular rough surface (MOMOI, 1980 b) and by a rectangular one (MOMOI, 1982) (these papers will be referred to as papers II and IV, respectively), we study in this paper the scattering of Rayleigh waves by a semi-circular rough surface on layered media. The method of analysis is the same as that used in papers II and IV. That is to say, the boundary is divided into a large number of small boundaries; the boundary condition is then represented by the quantities avaraged over each divided boundary. A set of the avaraged boundary conditions obtained in such a way are used as an infinite system of simultaneous equations which determine the behavior of the waves in the field in question. The same method is also used in the study on the scattering of edge water waves, which are analogous to Love waves in elastic media, due to semi-circular bay (MOMOI, 1981). The method developed in the above papers is rather similar to what is called *boundary element*

method (BREBBIA, 1978).

In this study, the effects of the semi-circular mountain on the partition of the energy of the scattered waves are elucidated in the case of the existence of the upper layer.

In the study concerning the edge waves, analogous to Love waves, in the continental shelf (MOMOI, 1976 b; this paper will be referred to as paper I), we have found the interesting feature that the existence of the edge waves of the leaky mode decreases the transmibility of the edge waves through the irregular coast of the estuary; In the present study concerning Rayleigh waves we will also find that the generation of the resonant standing P and S waves of leaky mode near the surface play very important roles on the transmission of Rayleigh waves through the semi-circular mountain.

2. Theory

2.1 Model used and equations

The model used in this paper is illustrated in Fig. 1. A semi-circular mountain range, with radius B, is located along the y-axis on a semi-infinite elastic body, which extend in the range $z \geqq 0$, with a layer (depth H) along the free surface. Incident Rayleigh waves travel along the x-axis from $x=-\infty$ toward the origin of the coordinates. It is assumed that the displacements in the incident waves lie in a plane perpendicular to the axis of the mountain range. The problem is, therefore, two-dimensional.

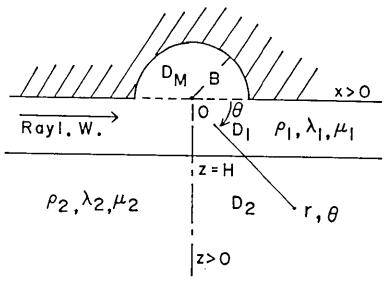

Fig. 1. Used model.

The entire portion of the elastic medium is partitioned into three domains, i.e., D_M is the domain in the range ($z \leqq 0$, $|r| \leqq B$), D_1 the domain ($H \geqq z \geqq 0$, $-\infty < x < +\infty$) and D_2 the domain ($z \geqq H$, $-\infty < x < +\infty$). Let (u_j, w_j) be the displacement component of the medium in domain D_j ($j=1, 2, M$) in the (x, z) directions. The equations of motion of the medium in the case of periodic motion are expressed by

$$\left(\frac{\partial^2}{\partial x^2}+\frac{\partial^2}{\partial z^2}+\begin{Bmatrix} h_j^2 \\ k_j^2 \end{Bmatrix}\right)\cdot\begin{Bmatrix} \phi_j \\ \psi_j \end{Bmatrix}=0 \ , \tag{1a}$$

$$u_j=\frac{\partial \phi_j}{\partial x}+\frac{\partial \psi_j}{\partial z} \ , \qquad w_j=\frac{\partial \phi_j}{\partial z}-\frac{\partial \psi_j}{\partial x} \ , \tag{1b}$$

$$h_j=\sigma\Big/\sqrt{\frac{\lambda_j+2\mu_j}{\rho_j}} \quad \text{and} \quad k_j=\sigma\Big/\sqrt{\frac{\mu_j}{\rho_j}}\,, \tag{1c}$$

where ρ_j is the density of the elastic medium in domain D_j, σ is the angular frequency in the time factor $e^{i\sigma t}$ (t: variable of time) and λ_j, μ_j Lame's constants. In a later development of the theory, Cartesian coordinates in (1a) will be transformed to polar coordinates (r, θ).

2.2 Conditions at the free surface and the interface

At the free surface ($z=0$) and the interface ($z=H$) conditions of the continuity of normal and tangential stresses $\{Z_z^{(j)}, X_z^{(j)}\}$ are given by

$$Z_z^{(1)}=X_z^{(1)}=0 \quad \text{for } |x|\geqq B \quad (z=0) \tag{2a}$$

and

$$X_z^{(1)}=X_z^{(2)}\,, \qquad Z_z^{(1)}=Z_z^{(2)}\,, \quad (z=H)\,, \tag{2b}$$

where

$$\left.\begin{aligned} X_z^{(j)}&=\mu_j\Big(\frac{\partial u_j}{\partial z}+\frac{\partial w_j}{\partial x}\Big)\,,\\ Z_z^{(j)}&=\lambda_j\frac{\partial u_j}{\partial x}+(\lambda_j+2\mu_j)\frac{\partial w_j}{\partial z}\,, \end{aligned}\right\} \quad (j=1,\,2)\,. \tag{2c}$$

On the cylindrical surface ($r=B$) radial and azimuthal stress components are expressed by

$$\left.\begin{aligned} R_R&=\frac{\lambda_1}{r}\Big\{\frac{\partial(rW)}{\partial r}+\frac{\partial U}{\partial\theta}\Big\}+2\mu_1\frac{\partial W}{\partial r}=0\,,\\ \Theta_R&=\mu_1\Big(\frac{\partial U}{\partial r}-\frac{U}{r}+\frac{1}{r}\frac{\partial W}{\partial\theta}\Big)=0\,, \end{aligned}\right\} \quad (r=B) \tag{3}$$

where U and W are azimuthal and radial components of displacement in the mountain, respectively.

Meanwhile, there exist conditions of the continuity of the displacement at the interface, i.e.

$$u_1=u_2\,, \qquad w_1=w_2\,, \quad (z=H)\,. \tag{4}$$

As described in Section 2.1 the part of the mountain and that of the upper layer are treated as separate domains. Artificial conditions are, therefore, required between these two domains. That is to say,

$$\left.\begin{aligned} u_M&=u_1\,, & w_M&=w_1\,,\\ X_z^{(M)}&=X_z^{(1)}\,, & Z_z^{(M)}&=Z_z^{(1)}\,, \end{aligned}\right\} \quad \text{for } |x|\leqq B \quad (z=0)\,. \tag{5}$$

2.3 Incident waves

Incident Rayleigh waves, which satisfy Eqs. (1a) and (1b) and the

boundary conditions at the surface and the interface given in § 2.1 in the case without any surface irregularity, are expressed as follows. The time factor $e^{i\sigma t}$ is then omitted as usual. This convention will be followed hereafter.

Let k_R and $(u_{jR}^{\text{in}}, w_{jR}^{\text{in}})$ be the wave number and the displacement components (u_j, w_j) of incident Rayleigh waves. The expressions of these waves in domain D_1 are given by

$$\left.\begin{aligned} u_{1R}^{\text{in}} &= U_{1R}^{\text{in}} \cdot e^{-ik_R x} \\ w_{1R}^{\text{in}} &= W_{1R}^{\text{in}} \cdot e^{-ik_R x} \end{aligned}\right\} \tag{6a}$$

with

$$\left.\begin{aligned} U_{1R}^{\text{in}} &= (C_1^{\phi} \cdot C_{\alpha_{1R}z} + S_1^{\phi} \cdot S_{\alpha_{1R}z})(-ik_R) \\ &\quad + (C_1^{\psi} \cdot S_{\beta_{1R}z} + S_1^{\psi} \cdot C_{\beta_{1R}z}) \cdot \beta_{1R} \\ W_{1R}^{\text{in}} &= (C_1^{\phi} \cdot S_{\alpha_{1R}z} + S_1^{\phi} \cdot C_{\alpha_{1R}z}) \cdot \alpha_{1R} \\ &\quad + (C_1^{\psi} \cdot C_{\beta_{1R}z} + S_1^{\psi} \cdot S_{\beta_{1R}z})(+ik_R) \end{aligned}\right\}, \tag{6b}$$

where

$$\left.\begin{aligned} &\alpha_{jR} = \sqrt{k_R^2 - h_j^2}\,, \qquad \beta_{jR} = \sqrt{k_R^2 - k_j^2}\,, \\ &S_{\gamma z} = \sinh \gamma z\,, \qquad C_{\gamma z} = \cosh \gamma z\,, \end{aligned}\right\} \tag{6c}$$

with

$$\gamma = \alpha_{jR} \quad \text{and} \quad \beta_{jR} \quad (j = 1, 2)\,.$$

Meanwhile, the expressions of incident Rayleigh waves in domain D_2 are given by

$$\left.\begin{aligned} u_{2R}^{\text{in}} &= U_{2R}^{\text{in}} \cdot e^{-ik_R x} \\ w_{2R}^{\text{in}} &= W_{2R}^{\text{in}} \cdot e^{-ik_R x} \end{aligned}\right\} \tag{7a}$$

with

$$\left.\begin{aligned} U_{2R}^{\text{in}} &= C_2^{\phi} \cdot (-ik_R) e^{-\alpha_{2R}\bar{z}} - C_2^{\psi} \cdot \beta_{2R} e^{-\beta_{2R}\bar{z}} \\ W_{2R}^{\text{in}} &= -C_2^{\phi} \cdot \alpha_{2R} e^{-\alpha_{2R}\bar{z}} + C_2^{\psi} \cdot (+ik_R) e^{-\beta_{2R}\bar{z}} \end{aligned}\right\} \tag{7b}$$

where

$$\bar{z} = z - H\,.$$

In (6b) and (7b), C_j^f and S_j^f $(j=1, 2$ and $f=\phi, \psi)$ are coefficients determined by the boundary conditions described in the previous section. These governing equations are expressed as follows.

Let A with a_{ij} $(i, j=1, 2\cdots, 6)$ as the elements be the matrix of the coefficients obtained from the conditions §2.2 in the case without any surface irregularity, and

$$C = (C_1^{\phi},\ S_1^{\phi},\ C_1^{\psi},\ S_1^{\psi},\ C_2^{\phi},\ C_2^{\psi})$$

be the vector of the unknown coefficients in the expressions (6b) and (7b).

By using the transposed vector C^t, we have equations

$$AC^t=0\ , \tag{8a}$$

where

$$a_{11}=1\ , \qquad a_{14}=f_{1R}(\beta)\ , \tag{8a, 1}$$

$$a_{22}=-f_{1R}(\alpha)\ , \qquad a_{23}=1\ . \tag{8a, 2}$$

$$\left.\begin{aligned} &a_{32}=S_{\alpha_{1R}H}+f_{1R}(\alpha)f_{1R}(\beta)\cdot S_{\beta_{1R}H}\ , \\ &a_{34}=f_{1R}(\beta)\cdot C_{\alpha\beta R}\ , \\ &a_{35}=-\bar{\bar{K}}_{21R}\ , \qquad a_{36}=\bar{\bar{K}}_{21R}\cdot f_{2R}(\beta)\ , \end{aligned}\right\} \tag{8a, 3}$$

$$\left.\begin{aligned} &a_{42}=f_{1R}(\alpha)\cdot C_{\alpha\beta R}\ , \\ &a_{44}=f_{1R}(\alpha)f_{1R}(\beta)\cdot S_{\alpha_{1R}H}+S_{\beta_{1R}H}\ , \\ &a_{45}=-\bar{\bar{K}}_{21R}\cdot f_{2R}(\alpha)\ , \qquad a_{46}=-\bar{\bar{K}}_{21R}\ , \end{aligned}\right\} \tag{8a, 4}$$

$$\left.\begin{aligned} &a_{52}=ik_R\cdot\left(-S_{\alpha_{1R}H}+\frac{2\alpha_{1R}\beta_{1R}}{\bar{\bar{K}}_{1R}}\cdot S_{\beta_{1R}H}\right) \\ &a_{54}=\beta_{1R}\cdot\left(-\frac{2k_R^2}{\bar{\bar{K}}_{1R}}\cdot C_{\alpha_{1R}H}+C_{\beta_{1R}H}\right) \\ &a_{55}=ik_R\ , \qquad a_{56}=\beta_{2R} \end{aligned}\right\} \tag{8a, 5}$$

$$\left.\begin{aligned} &a_{62}=\alpha_{1R}\cdot\left(C_{\alpha_{1R}H}-\frac{2k_R^2}{\bar{\bar{K}}_{1R}}\cdot C_{\beta_{1R}H}\right) \\ &a_{64}=ik_R\cdot\left(-\frac{2\alpha_{1R}\beta_{1R}}{\bar{\bar{K}}_{1R}}\cdot S_{\alpha_{1R}H}+S_{\beta_{1R}H}\right) \\ &a_{65}=\alpha_{2R}\ , \qquad a_{66}=-ik_R \end{aligned}\right\} \tag{8a, 6}$$

and

$$\text{the other coefficients}\quad a_{ij}=0 \tag{8a, 7}$$

with

$$\left.\begin{aligned} &f_{jR}(\gamma)=\frac{2ik_R\gamma_{jR}}{\bar{\bar{K}}_{jR}}\quad(\gamma=\alpha,\ \beta\ \text{and}\ j=1,\ 2)\ , \\ &C_{\alpha\beta R}=-C_{\alpha_{1R}H}+C_{\beta_{1R}H}\ , \qquad \bar{\bar{K}}_{21R}=\frac{\mu_2}{\mu_1}\cdot\frac{\bar{\bar{K}}_{2R}}{\bar{\bar{K}}_{1R}}\ , \\ &\bar{\bar{K}}_{jR}=2k_R^2-k_j^2\quad(j=1,\ 2)\ . \end{aligned}\right\} \tag{8a, 8}$$

The wave numbers k_R (generally, plural) of incident Rayleigh waves are the solution of the equation

$$|A|=0\ , \tag{8b}$$

where A is the coefficient matrix given in (8a).

The solutions are then readily obtained by use of the computer.

2.4 Expressions for displacement potentials of waves

Using the Fourier transform technique, the displacement potentials ϕ_j and ψ_j in D_j $(j=1, 2)$ satisfying Eq. (1a) are expressed by

$$\begin{Bmatrix}\phi_1\\ \psi_1\end{Bmatrix}=\frac{1}{\sqrt{2\pi}}\int_{-\infty}^{\infty}\begin{Bmatrix}\tilde{C}_1^{\phi}\cdot C_{\alpha_1 z}+\tilde{S}_1^{\phi}\cdot S_{\alpha_1 z}\\ \tilde{C}_1^{\psi}\cdot C_{\beta_1 z}+\tilde{S}_1^{\psi}\cdot S_{\beta_1 z}\end{Bmatrix}e^{+i\tilde{k}x}d\tilde{k} \tag{9a}$$

and

$$\begin{Bmatrix}\phi_2\\ \psi_2\end{Bmatrix}=\frac{1}{\sqrt{2\pi}}\int_{-\infty}^{\infty}\begin{Bmatrix}\tilde{C}_2^{\phi}\\ \tilde{C}_2^{\psi}\end{Bmatrix}\exp\left(i\tilde{k}x-\begin{Bmatrix}\alpha_2\\ \beta_2\end{Bmatrix}\bar{z}\right)d\tilde{k}\,, \tag{9b}$$

where

$$\bar{z}=Z-H\,,$$

$$\alpha_j=\sqrt{\tilde{k}^2-h_j^2}\,,\qquad \beta_j=\sqrt{\tilde{k}^2-k_j^2}\,,\quad (j=1, 2)\,, \tag{9c}$$

$S_{\gamma z}$ and $C_{\gamma z}$ (then $\gamma=\alpha_j, \beta_j$) are given in (6c), and $\{\tilde{C}_j^{\gamma}, \tilde{S}_j^{\gamma}\}$ $(\gamma=\phi, \psi)$ are unknown coefficients.

The branch cut of α_j (or β_j) runs from $\tilde{k}=\pm h_j$ (or $\pm k_j$) to $\pm(h_j-i\infty)$ (or $\pm(k_j-i\infty)$) on the complex plane.

The potentials ϕ_M anp ψ_M in the mountain are expressed by use of the Fourier expansion as

$$\begin{Bmatrix}\phi_M\\ \psi_M\end{Bmatrix}=\sum_n\left(\begin{Bmatrix}A_c^{(n)}\\ B_c^{(n)}\end{Bmatrix}\cos n\theta+\begin{Bmatrix}A_s^{(n)}\\ B_s^{(n)}\end{Bmatrix}\sin n\theta\right)\begin{Bmatrix}J_n(hr)\\ J_n(kr)\end{Bmatrix}\quad\text{in } D_M\,, \tag{9d}$$

where $A_j^{(n)}\cdot B_j^{(n)}$ $(j=c, s)$ are unknown coefficients, $J_n(z)$ the Bessel functions with the argument z, and $\sum_n$ the abbreviation for $\sum_{n=0}^{\infty}$. Expressions in the curly brackets are taken in the same order. This convention will be followed in the later discussions, unless otherwise stated.

2.5 Expressions for displacements of waves

Substituting (9a) and (9b) into (1b), we have the expressions for the displacements (u_j, w_j) of waves in domains D_j $(j=1, 2)$

$$\begin{Bmatrix}u_1\\ w_1\end{Bmatrix}=\frac{1}{\sqrt{2\pi}}\int_{-\infty}^{\infty}\left[\left(\tilde{C}_1^{\phi}\cdot\begin{Bmatrix}C_{\alpha_1 z}\\ S_{\alpha_1 z}\end{Bmatrix}+\tilde{S}_1^{\phi}\cdot\begin{Bmatrix}S_{\alpha_1 z}\\ C_{\alpha_1 z}\end{Bmatrix}\right)\begin{Bmatrix}i\tilde{k}\\ \alpha_1\end{Bmatrix}\right.$$
$$\left.+\left(\tilde{C}_1^{\psi}\cdot\begin{Bmatrix}S_{\beta_1 z}\\ C_{\beta_1 z}\end{Bmatrix}+\tilde{S}_1^{\psi}\cdot\begin{Bmatrix}C_{\beta_1 z}\\ S_{\beta_1 z}\end{Bmatrix}\right)\begin{Bmatrix}\beta_1\\ -i\tilde{k}\end{Bmatrix}\right]e^{+i\tilde{k}x}d\tilde{k} \tag{10a}$$

and

$$\begin{Bmatrix}u_2\\ w_2\end{Bmatrix}=\frac{1}{\sqrt{2\pi}}\int_{-\infty}^{\infty}\left[\tilde{C}_2^{\phi}\cdot\begin{Bmatrix}i\tilde{k}\\ -\alpha_2\end{Bmatrix}e^{-\alpha_2\bar{z}}-\tilde{C}_2^{\psi}\cdot\begin{Bmatrix}\beta_2\\ i\tilde{k}\end{Bmatrix}e^{-\beta_2\bar{z}}\right]e^{+i\tilde{k}x}d\tilde{k}\,. \tag{10b}$$

In the derivation of the azimuthal and radial displacement components (U, W) in domain D_M, the conversion of Cartesian coordinates in (1b) into the polar ones is required. These displacements are ex-

pressed by

$$\begin{Bmatrix} U \\ W \end{Bmatrix} = \frac{1}{r}\frac{\partial}{\partial\theta}\begin{Bmatrix} \phi_M \\ \psi_M \end{Bmatrix} + \frac{\partial}{\partial\theta}\begin{Bmatrix} -\psi_M \\ \phi_M \end{Bmatrix} . \tag{10c}$$

Substituting (9d) into (10c), we have expressions for the displacement in the mountain in polar coordinates as follows:

$$\left.\begin{aligned} U &= U_P + U_S \\ W &= W_P + W_S \end{aligned}\right\} , \tag{10d}$$

$$\begin{Bmatrix} U_P \\ W_P \end{Bmatrix} = \sum_n \left(A_c^{(n)} \begin{Bmatrix} \sin n\theta \\ \cos n\theta \end{Bmatrix} \mp A_s^{(n)} \begin{Bmatrix} \cos n\theta \\ \sin n\theta \end{Bmatrix} \right) \begin{Bmatrix} (-n)J_n^{hr}/r \\ hDJ_n^{hr} \end{Bmatrix} , \tag{10e}$$

and

$$\begin{Bmatrix} U_S \\ W_S \end{Bmatrix} = \sum_n \left(\pm B_c^{(n)} \begin{Bmatrix} \cos n\theta \\ \sin n\theta \end{Bmatrix} + B_s^{(n)} \begin{Bmatrix} \sin n\theta \\ \cos n\theta \end{Bmatrix} \right) \begin{Bmatrix} (-k)DJ_n^{kr} \\ nJ_n^{kr}/r \end{Bmatrix} , \tag{10f}$$

where (U_P, W_P) and (U_S, W_S) are dilatational and distortional wave components of (U, W), respectively, and $J_n^{\gamma r} = J_n(\gamma r)$, $DJ_n^{\gamma r} = \partial J_n(\gamma r)/\partial(\gamma r)$ $(\gamma = h \text{ or } k)$.

The displacements (u_M, w_M) in D_M in Cartesian coordinates are then given by

$$\begin{Bmatrix} u_M \\ w_M \end{Bmatrix} = \begin{Bmatrix} W \\ U \end{Bmatrix} \cos\theta \mp \begin{Bmatrix} U \\ W \end{Bmatrix} \sin\theta . \tag{10g}$$

By use of the conditions (2a), (2b), (4) and the second ones of (5) except the first ones, which will be used later, the expressions (10a) and (10b) are reduced to

$$\begin{Bmatrix} u_j \\ w_j \end{Bmatrix} = \frac{1}{\sqrt{2\pi}} \int_{-\infty}^{\infty} \begin{Bmatrix} U_j \\ W_j \end{Bmatrix} e^{+i\tilde{k}x} d\tilde{k} \quad (j = 1, 2) , \tag{11a}$$

where

$$\begin{aligned} U_1 = \frac{1}{\mu_1 \bar{\bar{K}}_1} \Big\{ & -\beta_1 \cdot \frac{\bar{\bar{S}}_1^{\psi}}{l^{\phi}} \cdot A_{u1}(\tilde{k}, z) + i\tilde{k} \cdot \frac{\bar{\bar{S}}_1^{\phi}}{l^{\phi}} \cdot B_{u1}(\tilde{k}, z) \\ & + (\beta_1 \cdot S_{\beta_1 z} \cdot \tilde{X}_z + i\tilde{k} \cdot C_{\alpha_1 z} \cdot \tilde{Z}_z) \Big\} , \end{aligned} \tag{11b}$$

$$\begin{aligned} W_1 = \frac{1}{\mu_1 \bar{\bar{K}}_1} \Big\{ & -i\tilde{k} \cdot \frac{\bar{\bar{S}}_1^{\psi}}{l^{\phi}} \cdot A_{w1}(\tilde{k}, z) + \alpha_1 \cdot \frac{\bar{\bar{S}}_1^{\phi}}{l^{\phi}} \cdot B_{w1}(\tilde{k}, z) \\ & + (-i\tilde{k} \cdot C_{\beta_1 z} \cdot \tilde{X}_z + \alpha_1 \cdot S_{\alpha_1 z} \cdot \tilde{Z}_z) \Big\} , \end{aligned} \tag{11c}$$

$$\left.\begin{aligned} A_{u1}(\tilde{k}, z) &= \frac{-2\tilde{k}^2}{\bar{\bar{K}}_1} \cdot C_{\alpha_1 z} + C_{\beta_1 z} \\ B_{u1}(\tilde{k}, z) &= S_{\alpha_1 z} - \frac{2\alpha_1\beta_1}{\bar{\bar{K}}_1} \cdot S_{\beta_1 z} \end{aligned}\right\} , \tag{11d}$$

$$\left.\begin{aligned} A_{w1}(\tilde{k},\, z)&=\frac{2\alpha_1\beta_1}{\bar{\bar{K}}_1}\cdot S_{\alpha_1 z}-S_{\beta_1 z}\\ B_{w1}(\tilde{k},\, z)&=C_{\alpha_1 z}-\frac{2\tilde{k}^2}{\bar{\bar{K}}_1}\cdot C_{\beta_1 z}\end{aligned}\right\}, \tag{11e}$$

$$\begin{Bmatrix} U_2\\ W_2\end{Bmatrix}=\begin{Bmatrix} U_2^P\\ W_2^P\end{Bmatrix}e^{-\alpha_2\bar{z}}+\begin{Bmatrix} U_2^S\\ W_2^S\end{Bmatrix}e^{-\beta_2\bar{z}}\quad(\bar{z}=z-H)\,, \tag{11f}$$

$$\begin{Bmatrix} U_2^P\\ W_2^P\end{Bmatrix}=\frac{1}{V_H\mu_1\bar{\bar{K}}_1}\Big\{(-a_{sc}-f_1(\alpha)\cdot b_{cs})\cdot\frac{\bar{\bar{S}}_1^{\phi}}{l^{\phi}}+(-b_{sc}+f_1(\beta)\cdot a_{cs})\cdot\frac{\bar{\bar{S}}_1^{\psi}}{l^{\phi}}$$
$$+(-a_{cs}\cdot\tilde{Z}_z+b_{cs}\cdot\tilde{X}_z)\Big\}\begin{Bmatrix} i\tilde{k}\\ -\alpha_2\end{Bmatrix}\,, \tag{11g}$$

$$\begin{Bmatrix} U_2^S\\ W_2^S\end{Bmatrix}=\frac{1}{V_H\mu_1\bar{\bar{K}}_1}\Big\{(-e_{sc}+f_1(\alpha)\cdot f_{cs})\cdot\frac{\bar{\bar{S}}_1^{\phi}}{l^{\phi}}+(f_{sc}+f_1(\beta)\cdot e_{cs})\cdot\frac{\bar{\bar{S}}_1^{\psi}}{l^{\phi}}$$
$$-(e_{cs}\cdot\tilde{Z}_z+f_{cs}\cdot\tilde{X}_z)\Big\}\begin{Bmatrix} -\beta_2\\ -i\tilde{k}\end{Bmatrix}\,, \tag{11h}$$

$$\begin{Bmatrix} \tilde{X}_z\\ \tilde{Z}_z\end{Bmatrix}=\frac{1}{\sqrt{2\pi}}\int_{-B}^{B}\begin{Bmatrix} X_z^{(M)}|_{z=0}\\ Z_z^{(M)}|_{z=0}\end{Bmatrix}e^{-i\tilde{k}x}dx\,, \tag{11i}$$

$$\left.\begin{aligned} f_1(\gamma)&=\frac{2i\tilde{k}\gamma_1}{\bar{\bar{K}}_1}\quad(\gamma=\alpha,\,\beta)\,,\qquad \bar{\bar{K}}_j=2\tilde{k}^2-k_j^2\quad(j=1,\,2)\,,\\ V_H&=\alpha_2\beta_2-\tilde{k}^2\,,\end{aligned}\right\} \tag{11j}$$

$$\bar{\bar{S}}_1^{\bar{\gamma}}=(\gamma_{cs}\cdot i^{\bar{\gamma}}-p_{cs}\cdot j^{\bar{\gamma}})\cdot\tilde{Z}_z+(s_{cs}\cdot i^{\bar{\gamma}}-q_{cs}\cdot j^{\bar{\gamma}})\cdot\tilde{X}_z \tag{11k}$$

with $\bar{\gamma}=\phi$ and ψ for $\gamma=\psi$ and ϕ, respectively,

$$\left.\begin{aligned} i^{\phi}&=-f_1(\alpha)\cdot q_{cs}+p_{sc}\,,\qquad j^{\phi}=-f_1(\alpha)\cdot s_{cs}+\gamma_{sc}\,,\\ i^{\psi}&=+f_1(\beta)\cdot p_{cs}+q_{sc}\,,\qquad j^{\psi}=+f_1(\beta)\cdot\gamma_{cs}+s_{sc}\,,\end{aligned}\right\} \tag{11l}$$

$$\left.\begin{aligned} p_{\Gamma}&=c_{\Gamma}+f_H\cdot a_{\Gamma}\,,\qquad q_{\Gamma}=-d_{\Gamma}-f_H\cdot b_{\Gamma}\,,\\ r_{\Gamma}&=g_{\Gamma}+f_H\cdot e_{\Gamma}\,,\qquad s_{\Gamma}=h_{\Gamma}+f_H\cdot f_{\Gamma}\,,\end{aligned}\right\}\quad(\Gamma=cs,\,sc) \tag{11m}$$

with

$$f_H=\frac{\mu_2}{\mu_1}\cdot\frac{1}{V_H}(\bar{\bar{K}}_2^2-4\tilde{k}^2\alpha_2\beta_2)\,,$$

$$\left.\begin{aligned} a_{\xi\eta}&=\xi_{\alpha_1 H}\tilde{k}^2+\eta_{\alpha_1 H}\alpha_1\beta_2\,,\qquad b_{\xi\eta}=(\eta_{\beta_1 H}\beta_1+\xi_{\beta_1 H}\beta_2)\cdot i\tilde{k}\,,\\ c_{\xi\eta}&=\bar{\bar{K}}_1\bar{\bar{K}}_2\xi_{\alpha_1 H}+4\tilde{k}^2\alpha_1\beta_2\eta_{\alpha_1 H}\,,\qquad d_{\xi\Gamma}=(\beta_2\bar{\bar{K}}_1\xi_{\beta_1 H}+\beta_1\bar{\bar{K}}_2\eta_{\beta_1 H})\cdot 2i\tilde{k}\,,\\ e_{\xi\eta}&=(\xi_{\alpha_1 H}\alpha_2+\eta_{\alpha_1 H}\alpha_1)^{*}i\tilde{k}\,,\qquad f_{\xi\Gamma}=\xi_{\beta_1 H}\tilde{k}^2+\eta_{\beta_1 H}\alpha_2\beta_1\,,\\ g_{\xi\eta}&=(\alpha_2\bar{\bar{K}}_1\xi_{\alpha_1 H}+\alpha_1\bar{\bar{K}}_2\eta_{\alpha_1 H})\cdot 2i\tilde{k}\,,\qquad h_{\xi\Gamma}=\bar{\bar{K}}_1\bar{\bar{K}}_2\xi_{\beta_1 H}+4\tilde{k}^2\alpha_2\beta_1\eta_{\beta_1 H}\,,\end{aligned}\right\} \tag{11n}$$

with $\xi=C$ and S for $\eta=S$ and C, respectively, and finally

$$l^{\phi}=i^{\phi}\cdot j^{\psi}-j^{\phi}\cdot i^{\psi}\,. \tag{11o}$$

In (11n), $\xi_{\Gamma H}$ with $\xi=C$ or S, for instance, indicates $C_{\Gamma H}=\cosh\gamma H$

or $S_{rH}=\sinh\gamma H$ by use of (6c).

Substituting (10g) into the second conditions in (5), we have

$$\left\{\frac{X_z^{(M)}}{\mu_1}\right\}_{z=0}=\bar{\bar{X}}=\sum_n A_s^{(n)}h_1^2\left\{-\frac{2(n-n^2)}{(h_1x)^2}J_n(h_1x)-\frac{2n}{h_1x}J_{n+1}(h_1x)\right\}$$
$$+\sum_n B_c^{(n)}k_1^2\left[\left\{\frac{2(n-n^2)}{(k_1x)^2}+1\right\}J_n(k_1x)-\frac{2}{k_1x}J_{n+1}(k_1x)\right] \quad (12a)$$

and

$$\left\{\frac{Z_z^{(M)}}{\mu_1}\right\}_{z=0}=\bar{\bar{Z}}=\sum_n A_c^{(n)}h_1^2\left[\left\{\frac{2(n-n^2)}{(h_1x)^2}-\frac{\lambda_1}{\mu_1}\right\}J_n(h_1x)-\frac{2}{h_1x}J_{n+1}(h_1x)\right]$$
$$+\sum_n B_s^{(n)}k_1^2\left\{\frac{2(n-n^2)}{(k_1x)^2}J_n(k_1x)+\frac{2n}{k_1x}J_{n+1}(k_1x)\right\}. \quad (12b)$$

In the integrals (11i) some approximation is introduced here. The integrals (11i) are expressed by the sum of each integral with small interval $x_q-\Delta x<x<x_q+\Delta x$ (q: from $-M$ to M excluding $q=0$), where $B=2M\Delta x$ and x_q is the midpoint of each interval. If the Bessel functions included in $X_z^{(M)}$ and $Z_z^{(M)}$ are approximately expressed by the value at the reference point x_q of the small interval, the integrals (11i) are reduced to

$$\frac{1}{\mu}\begin{Bmatrix}\tilde{X}_z\\ \tilde{Z}_z\end{Bmatrix}=\sqrt{\frac{2}{\pi}}\sum_{q=-M}^{M}{}'\begin{Bmatrix}\bar{\bar{X}}_z\\ \bar{\bar{Z}}_z\end{Bmatrix}_q\frac{\sin\tilde{k}\Delta x}{\tilde{k}}e^{-i\tilde{k}x_q}, \quad (12c)$$

where $\sum'$ with a prime indicates the summation of q from $-M$ to M excluding $q=0$ and $\{\bar{\bar{X}}, \bar{\bar{Z}}\}_q$ are the values of $\{X, Z\}$ at $x=x_q$.

2.6 Infinite system of simultaneous equations

In papers II (1980 b), III (1981) and IV (1982), the author introduced a paticular technique. Namely, boundaries are divided into a sequence of numerous smaller divisions in each of which the mean value is taken as representative value of the divided smaller boundary. Using this procedure, the system of simultaneous equations will be obtained in this paper.

The boundaries $\{-B\leqq x\leqq 0\}$ and $\{0\leqq x\leqq B\}$ at $z=0$ are divided, respectively, into M small intervals (width $2\Delta x$) with a reference point at its midpoint. The reference points are then expressed as $x_p=\pm(2p+1)\Delta x$ ($p=0, 1, 2, \cdots, M-1$) with $\Delta x=B/(2M)$. The sign $\pm$ is to be taken in the same order.

In the reduction of the foregoing section, the first condition of (5) associated with the continuity of the displacements at $z=0$ was not used. In order to obtain the solution, the use of this condition is required. Taking the mean value of this condition in each small interval, we have the set of conditions:

$$\left\{\int_{x_p-\Delta x}^{x_p+\Delta x}\begin{Bmatrix}u_1+u_{1R}^{\text{in}}\\ w_1+w_{1R}^{\text{in}}\end{Bmatrix}dx=\int_{x_p-\Delta x}^{x_p+\Delta x}\begin{Bmatrix}u_M\\ w_M\end{Bmatrix}dx \quad (z=0)\right.$$

$$\left.\text{for } p \text{ from } -M \text{ to } -1 \text{ and from 1 to } M \text{ } (4M \text{ eqs.})\right\} . \quad (13a)$$

By taking the mean value of (11a) ($j=1$) in each division, the first expressions of (13a) are reduced to

$$\int_{x_p-\Delta x}^{x_p+\Delta x}\begin{Bmatrix}u_1\\ w_1\end{Bmatrix}_{z=0}dx=\frac{1}{2\pi}\sum_{q=-M}^{M}{}'\left[\bar{\bar{Z}}_q\cdot\begin{Bmatrix}U_{q,p}^{\psi}\\ U_{q,p}^{\phi}\end{Bmatrix}+\bar{\bar{X}}_q\cdot\begin{Bmatrix}W_{q,p}^{\psi}\\ W_{q,p}^{\phi}\end{Bmatrix}\right], \quad (13b)$$

$$\begin{Bmatrix}U_{q,p}^{\gamma}\\ W_{q,p}^{\gamma}\end{Bmatrix}=\int_{-\infty}^{\infty}\begin{Bmatrix}M^{\gamma}\\ N^{\gamma}\end{Bmatrix}\cdot\tilde{R}_qR_p\,d\tilde{k} , \quad (13c)$$

$$\begin{Bmatrix}R_p\\ \tilde{R}_q\end{Bmatrix}=\exp\left(\pm i\tilde{k}\begin{Bmatrix}x_p\\ x_q\end{Bmatrix}\right)\cdot\frac{2\sin\tilde{k}\Delta x}{\tilde{k}} , \quad (13d)$$

$$\left.\begin{aligned}M^{\phi}&=\frac{1}{\bar{\bar{K}}_1}\cdot\tilde{K}_1\alpha_1\cdot m^{\phi} , \qquad M^{\psi}=\frac{1}{\bar{\bar{K}}_1}(\tilde{K}_1\beta_1\cdot m^{\psi}+i\tilde{k}) ,\\ N^{\phi}&=\frac{1}{\bar{\bar{K}}_1}(\tilde{K}_1\alpha_1\cdot n^{\phi}-i\tilde{k}) , \qquad N^{\psi}=\frac{1}{\bar{\bar{K}}_1}\cdot\tilde{K}_1\beta_1\cdot n^{\psi} ,\end{aligned}\right\} \quad (13e)$$

with

$$\left.\begin{aligned}\tilde{K}&=\frac{-k_1^2}{\bar{\bar{K}}_1} ,\\ m^{\gamma}&=\frac{1}{l^{\gamma}}(r_{cs}\cdot i^{\bar{\gamma}}-p_{cs}\cdot j^{\bar{\gamma}}) ,\\ n^{\gamma}&=\frac{1}{l^{\gamma}}(s_{cs}\cdot i^{\bar{\gamma}}-q_{cs}\cdot j^{\bar{\gamma}}) ,\end{aligned}\right\} \quad (13f)$$

with $l^{\psi}=-l^{\phi}$ and $\gamma=\{\phi, \psi\}$ for $\bar{\gamma}=\{\psi, \phi\}$, respectively.

In the above expressions $\{\bar{\bar{X}}_q, \bar{\bar{Z}}_q\}$ are given by (12a) and (12b) with the substitution of x_q for x. In the actual computation, the integrals (13c) are carried out by use of Simpson's formula with the help of the computer.

By taking the mean value of (6a) in each small interval the second expressions of (13a) are reduced to

$$\int_{x_p-\Delta x}^{x_p+\Delta x}\begin{Bmatrix}u_{1R}^{\text{in}}\\ w_{1R}^{\text{in}}\end{Bmatrix}_{z=0}dx=\begin{Bmatrix}U_{1R}^{\text{in}}\\ W_{1R}^{\text{in}}\end{Bmatrix}_{z=0}\cdot R_p\Big|_{\tilde{k}=-k_R} , \quad (13g)$$

where $\{u_{1R}^{\text{in}}, w_{1R}^{\text{in}}\}_{z=0}$ and R_p are given by (6a) and the first expression of (13d), respectively.

By taking the mean value of (10g) in each small interval, the right-hand side of (13a) becomes

$$\int_{x_p-\Delta x}^{x_p+\Delta x}\begin{Bmatrix}u_M\\ w_M\end{Bmatrix}_{z=0}dx=\sum_n\begin{Bmatrix}A_c^{(n)}\,dJ_n(h_1x_p)/dx_p+B_s^{(n)}nJ_n(k_1x_p)/x_p\\ A_s^{(n)}nJ_n(h_1x_p)/x_p-B_c^{(n)}\,dJ_n(k_1x_p)/dx_p\end{Bmatrix}\cdot 2\Delta x . \quad (13h)$$

In the reduction of the above expression, the Bessel function in the small intervals $\{x_p-\Delta x<x<x_p+\Delta x\}$ is approximated by the value at the midpoints x_p. If the width of the interval is small, this approximation is permissible.

The medium-free boundaries C_- and C_+ ($\pi\leqq\theta\leqq 3\pi/2$ and $3\pi/2\leqq\theta\leqq 2\pi$) in the semi-circular mountain are divided, respectively, into N intervals with width $2B\Delta\theta$ ($\fallingdotseq 2\Delta x$), where the reference point of the interval is located at the midpoint of each interval. The reference points are then expressed by $\theta_p=-\pi/2\pm(2p+1)\Delta\theta$ with p from 0 to $(N-1)$ in $C_\pm$, respectively. Taking the mean value of the condition (3) in each interval, we have the set of conditions:

$$\left\{\frac{1}{\mu_1}\int_{\theta_p-\Delta\theta}^{\theta_p+\Delta\theta}\begin{Bmatrix}R_R\\ \Theta_R\end{Bmatrix}_{r=b}d\theta=0\right.$$

$$\left.\text{for } p \text{ from } -N \text{ to } -1 \text{ and from 1 to } N\ (4N \text{ eqs.})\right\}. \tag{14a}$$

By taking the mean value of (3) after the substitution of (10d) into (3), we have

$$\frac{1}{\mu_1}\int_{\theta_p-\Delta\theta}^{\theta_p+\Delta\theta}R_R d\theta=\sum_n (A_c^{(n)}C_p^{(n)}+A_s^{(n)}S_p^{(n)})R_A^{(n)}h_1^2 + \sum_n (-B_c^{(n)}S_p^{(n)}+B_s^{(n)}C_p^{(n)})R_B^{(n)}k_1^2\,, \tag{14b}$$

with

$$\left\{\begin{aligned} R_A^{(n)}&=\left\{\frac{2(n^2-n)}{(k_1B)^2}-\left(\frac{\lambda_1}{\mu_1}+2\right)\right\}J_n^h+\frac{2J_{n+1}^h}{h_1B}\\ R_B^{(n)}&=2(n^2-n)\frac{J_n^k}{(k_1B)^2}-\frac{2nJ_{n+1}^k}{k_1B}\end{aligned}\right\}, \tag{14c}$$

and

$$\frac{1}{\mu_1}\int_{\theta_p-\Delta\theta}^{\theta_p+\Delta\theta}\Theta_R d\theta=\sum_n (-A_c^{(n)}S_p^{(n)}+A_s^{(n)}C_p^{(n)})\Theta_A^{(n)}h_1^2 + \sum_n (B_c^{(n)}C_p^{(n)}+B_s^{(n)}S_p^{(n)})\Theta_B^{(n)}k_1^2\,, \tag{14d}$$

with

$$\left\{\begin{aligned} \Theta_A^{(n)}&=2(n^2-n)\frac{J_n^h}{(h_1B)^2}-\frac{2nJ_{n+1}^h}{h_1B}\\ \Theta_B^{(n)}&=\left\{-\frac{2(n^2-n)}{(k_1B)^2}+1\right\}J_n^k-\frac{2J_{n+1}^k}{k_1B}\end{aligned}\right\}, \tag{14e}$$

where p covers the integers from $-N$ to -1 and from 1 to N,

$$\begin{Bmatrix}C_p^{(n)}\\ S_p^{(n)}\end{Bmatrix}=\begin{Bmatrix}\cos n\theta_p\\ \sin n\theta_p\end{Bmatrix}\cdot\frac{2\sin n\Delta\theta}{n}\,, \tag{14f}$$

and J_n^h or $J_n^k=J_n(h_1B)$ or $J_n(k_1B)$.

We have now arrived at the infinite system of simultaneous equations (13a) ($4M$ eqs.) and (14a) ($4N$ eqs.). These equations determine the $4(N_{\rm up}+1)$ unknown coefficients $\{A_C^{(n)}, B_C^{(n)}\ (n=0 \text{ to } N_{\rm up})\}$ and $\{A_s^{(n)}, B_s^{(n)}\ (n=1 \text{ to } N_{\rm up}+1)\}$. The number of the uppermost term $N_{\rm up}$ is given by the relation $4(M+N)=4(N_{\rm up}+1)$, where the left-hand side of this relation indicates the number of the equations given by (13a) and (14a).

2.7 Expressions for generated Rayleigh waves

The generated Rayleigh waves are given by the pole contribution of (11a). Let $\{u_{jGR}^{+}, w_{jGR}^{+}\}$ and $\{u_{jGR}^{-}, w_{jGR}^{-}\}$ be the generated transmitted, reflected Rayleigh waves in the domains D_j ($j=1, 2$), respectively, where suffix GR is the abbreviation of *Generated Rayleigh Waves*.

The (resultant) scattered transmitted $\{u_{jR}^{+}, w_{jR}^{+}\}$ and reflected $\{u_{jR}^{-}, w_{jR}^{-}\}$ Rayleigh waves in the domains D_j ($j=1, 2$) are expressed as

$$\begin{Bmatrix} u_{jR}^{+} \\ w_{jR}^{+} \end{Bmatrix} = \begin{Bmatrix} u_{jR}^{\rm in} \\ w_{jR}^{\rm in} \end{Bmatrix} + \begin{Bmatrix} u_{jGR}^{+} \\ w_{jGR}^{+} \end{Bmatrix} \tag{15a}$$

$$\begin{Bmatrix} u_{jR}^{-} \\ w_{jR}^{-} \end{Bmatrix} = \begin{Bmatrix} u_{jGR}^{-} \\ w_{jGR}^{-} \end{Bmatrix} . \tag{15b}$$

By using integrals (11a), the generated Rayleigh waves are expressed as

$$\begin{Bmatrix} u_{jGR}^{\pm} \\ w_{jGR}^{\pm} \end{Bmatrix} = \begin{Bmatrix} U_{jR}^{\pm} \\ W_{jR}^{\pm} \end{Bmatrix} \cdot e^{\mp ik_R x} \quad (j=1, 2) , \tag{16a}$$

where

$$U_{1R}^{\pm} = \frac{\sqrt{2\pi}}{\mu_1 \bar{\bar{K}}_{1R}} \cdot \frac{i}{\{dl^{\phi}/d\tilde{k}\}_{\tilde{k}=k_R}} \cdot \{\beta_{1R} \cdot A_{u1}(k_R, z) \cdot \bar{\bar{S}}_1^{\psi}|_{\tilde{k}=\mp k_R} \pm ik_R \cdot B_{u1}(k_R, z) \cdot \bar{\bar{S}}_1^{\phi}|_{\tilde{k}=\mp k_R}\} , \tag{16b}$$

$$W_{1R}^{\pm} = \frac{\sqrt{2\pi}}{\mu_1 \bar{\bar{K}}_{1R}} \cdot \frac{i}{\{dl^{\phi}/d\tilde{k}\}_{\tilde{k}=k_R}} \cdot \{\mp ik_R \cdot A_{w1}(k_R, z) \cdot \bar{\bar{S}}_1^{\psi}|_{\tilde{k}=\mp k_R} - \alpha_{1R} \cdot B_{w1}(k_R, z) \cdot \bar{\bar{S}}_1^{\phi}|_{\tilde{k}=\mp k_R}\} , \tag{16c}$$

$$\begin{Bmatrix} U_{2R}^{\pm} \\ W_{2R}^{\pm} \end{Bmatrix} = \begin{Bmatrix} \mp ik_R \\ -\alpha_{2R} \end{Bmatrix} \cdot \bar{\bar{C}}_{2R}^{\phi} \cdot e^{-\alpha_{2R}\tilde{z}} + \begin{Bmatrix} -\beta_{2R} \\ \pm ik_R \end{Bmatrix} \cdot \bar{\bar{C}}_{2R}^{\psi} \cdot e^{-\beta_{2R}\tilde{z}} , \tag{16d}$$

$$\bar{\bar{C}}_{2R}^{\phi} = \frac{\sqrt{2\pi}}{V_{HR} \cdot \mu_1 \bar{\bar{K}}_{1R}} \cdot \frac{i}{\{dl^{\phi}/d\tilde{k}\}_{\tilde{k}=k_R}} \cdot \{(a_{sc}+f_1(\alpha) \cdot b_{cs}) \cdot \bar{\bar{S}}_1^{\phi} + (b_{sc}-f_1(\beta) \cdot a_{cs}) \cdot \bar{\bar{S}}_1^{\psi}\}_{\tilde{k}=\mp k_R} , \tag{16e}$$

$$\bar{\bar{C}}_{2R}^{\psi} = \frac{\sqrt{2\pi}}{V_{HR} \cdot \mu_1 \bar{\bar{K}}_{1R}} \cdot \frac{i}{\{dl^{\phi}/d\tilde{k}\}_{\tilde{k}=k_R}} \cdot \{(e_{sc}-f_1(\alpha) \cdot f_{cs}) \cdot \bar{\bar{S}}_1^{\phi} + (-f_{sc}-f_1(\beta) \cdot e_{cs}) \cdot \bar{\bar{S}}_1^{\psi}\}_{\tilde{k}=\mp k_R} , \tag{16f}$$

$$\{V_{HR}=V_H,\ \bar{\bar{K}}_{1R}=\bar{\bar{K}}_1\} \quad \text{with } \tilde{k}=k_R\ . \tag{16g}$$

In the expressions from (16b) to (16f), the derivative $\{dl^{\phi}/dk\}$ is replaced by $\delta l^{\phi}/\delta k$ with $\delta k=0.001$ in the actual computation. The computation of this derivative was carried out in double precision or 14 decimal digits.

2.8 Expressions for the waves scattered into the semi-infinite body

Changing the variable in the integrals (11a) from k to ξ by the expression $k=\{h_2 \text{ or } k_2\}\sin\xi$ for $\{P \text{ or } S\}$ waves, respectively, and using polar coordinates, we have the following expressions for the waves scattered into the semi-infinite body (domain D_2).

$$\begin{Bmatrix} u_2 \\ w_2 \end{Bmatrix} = \begin{Bmatrix} u_2^p \\ w_2^p \end{Bmatrix} + \begin{Bmatrix} u_2^s \\ w_2^s \end{Bmatrix}$$

with

$$\begin{Bmatrix} u_2^j \\ w_2^j \end{Bmatrix} = \int \begin{Bmatrix} G_u^j(\xi) \\ G_w^j(\xi) \end{Bmatrix} \exp\left[i\{h_2 \text{ or } k_2\}\bar{r}\sin(\xi-\bar{\theta})\right] d\xi \quad (j=P \text{ or } S)\ ,$$

where the path of the integration runs from $-\pi/2-i\infty$ to $-\pi/2$, from $-\pi/2$ to $+\pi/2$ and from $+\pi/2$ to $+\pi/2+i\infty$, and further, $\{G_u^j(\xi),\ G_w^j(\xi)\}$ are the integrands after the change of the variables and $x=\bar{r}\cos\bar{\theta}$, $z-H=\bar{r}\sin\bar{\theta}$.

Applying the saddle point method for large $\bar{r}$, we can obtain the expressions of the displacements $\{u_2,\ w_2\}$ at a great distance. Azimuthal (U) and radial (W) displacement components at a distance in the semi-infinite elastic body become

$$\begin{Bmatrix} U \\ W \end{Bmatrix} = \begin{Bmatrix} \dfrac{ik_2^2}{\sqrt{k_2\bar{r}}}\cdot\tilde{U}(\bar{\theta}) \\ \dfrac{-ih_2^2}{\sqrt{h_2\bar{r}}}\cdot\tilde{W}(\bar{\theta}) \end{Bmatrix} \cdot \exp\left(-i\begin{Bmatrix} k_2 \\ h_2 \end{Bmatrix}\bar{r}+i\pi/4\right)\ , \tag{17a}$$

$$\begin{Bmatrix} \tilde{U}(\bar{\theta}) \\ \tilde{W}(\bar{\theta}) \end{Bmatrix} = \begin{Bmatrix} U_2^s/(-\beta_2) \\ U_2^p/(i\tilde{k}) \end{Bmatrix} \cdot \sin\bar{\theta} \quad \text{with} \quad \tilde{k}=-\begin{Bmatrix} k_2 \\ h_2 \end{Bmatrix}\cdot\cos\bar{\theta}\ , \tag{17b}$$

where $\{U_2^p,\ U_2^s\}$ are given by {(11g), (11h)}, respectively.

2.9 Expressions for energy fluxes

The energy E transmitted across the surface, with a unit width along the y-axis, over one cycle in time is expressed as

$$E=\int_c ds\int_0^T dt\left(X_c\frac{du_c}{dt}+Z_c\frac{dw_c}{dt}\right)\ , \tag{18a}$$

where c, path of the integration; ds, infinitesimal along path c; T, period; X and Z, normal and tangential stresses on path c; u and w,

normal and tangential displacement components on path c. In the above the real parts of X_c, Z_c, u_c and w_c are considered.

Energy flux of the incident Rayleigh waves is first considered. Path c runs along the z-axis from $z=0$ to ∞ and $\{X_c, Z_c\}$ are given by

$$\{(\lambda+2\mu)\partial u_c/\partial x+\lambda\partial w_c/\partial z,\ \mu(\partial w_c/\partial x+\partial u_c/\partial z)\} \tag{18b}$$

with

$$\{u_c, w_c\}=\mathrm{Re}\,\{u_{jR}^{\mathrm{in}}e^{i\sigma t}, w_{jR}^{\mathrm{in}}e^{i\sigma t}\}\ .$$

Substituting (6a) and (7a) into (18a), we have the expression for the energy flux of the incident Rayleigh waves as follows:

$$E_R^{\mathrm{in}}=\int_0^H \delta E_{1R}^{\mathrm{in}}dz+\int_H^\infty \delta E_{2R}^{\mathrm{in}}dz\ , \tag{19a}$$

$$\delta E_{jR}^{\mathrm{in}}=\pi\{|X_{jR}^{\mathrm{in}}||U_{jR}^{\mathrm{in}}|\sin(\theta_{jR}^{X}-\theta_{jR}^{u})+|Z_{jR}^{\mathrm{in}}||W_{jR}^{\mathrm{in}}|\sin(\theta_{jR}^{Z}-\theta_{jR}^{w})\}\ , \tag{19b}$$

$$\left.\begin{aligned} X_{jR}^{\mathrm{in}}&=|X_{jR}^{\mathrm{in}}|\cdot e^{i\theta_{jR}^{X}(z)} \\ Z_{jR}^{\mathrm{in}}&=|Z_{jR}^{\mathrm{in}}|\cdot e^{i\theta_{jR}^{Z}(z)} \end{aligned}\right\},\qquad \left.\begin{aligned} U_{jR}^{\mathrm{in}}&=|U_{jR}^{\mathrm{in}}|\cdot e^{i\theta_{jR}^{u}(z)} \\ W_{jR}^{\mathrm{in}}&=|W_{jR}^{\mathrm{in}}|\cdot e^{i\theta_{jR}^{w}(z)} \end{aligned}\right\}, \tag{19c}$$

and there exist the relations

$$\left.\begin{aligned} X_{jR}^{\mathrm{in}}&=\lambda_j\cdot\frac{dW_{jR}^{\mathrm{in}}}{dz}+(\lambda_j+2\mu_j)(-ik_R)U_{jR}^{\mathrm{in}} \\ Z_{jR}^{\mathrm{in}}&=\mu_j\left(-ik_RW_{jR}^{\mathrm{in}}+\frac{dU_{jR}^{\mathrm{in}}}{dz}\right) \end{aligned}\right\}, \tag{19d}$$

where $\{U_{jR}^{\mathrm{in}}, W_{jR}^{\mathrm{in}}\}$ $(j=1, 2)$ are given by (6b) and (7b).

Likewise, for the scattered Rayleigh waves, the path c and the expression of the stress (i.e., (18b)) are the same as those in the case of the incident Rayleigh waves.

Substituting (15a) and (15b) into (18a), we have the following expressions for the energy flux of the transmitted and reflected Rayleigh waves: E_{jR}^{γ} $(\gamma=\mathrm{tr}$ and $\mathrm{re})$, in the domains D_j $(j=1, 2)$, respectively.

$$E_R^{\gamma}=E_{1R}^{\gamma}+E_{2R}^{\gamma}\quad(\gamma=\mathrm{tr},\ \mathrm{re}) \tag{20a}$$

$$\left\{\begin{matrix} E_{1R}^{\gamma} \\ E_{2R}^{\gamma} \end{matrix}\right\}=\left\{\begin{matrix} \int_0^H \delta E_{1R}^{\gamma} \\ \int_H^\infty \delta E_{2R}^{\gamma} \end{matrix}\right\}dz\ , \tag{20b}$$

$$\delta E_{jR}^{\gamma}=\pi\{|\tilde{X}_{jR}^{\pm}||\tilde{U}_{jR}^{\pm}|\sin(\theta_{jR}^{X\pm}-\theta_{jR}^{u\pm})+|\tilde{Z}_{jR}^{\pm}||\tilde{W}_{jR}^{\pm}|\sin(\theta_{jR}^{Z\pm}-\theta_{jR}^{w\pm})\}\ , \tag{20c}$$

$$\left.\begin{aligned} \tilde{X}_{jR}^{\pm}&=|\tilde{X}_{jR}^{\pm}|\cdot e^{i\theta_{jR}^{X\pm}(z)} \\ \tilde{Z}_{jR}^{\pm}&=|\tilde{Z}_{jR}^{\pm}|\cdot e^{i\theta_{jR}^{Z\pm}(z)} \end{aligned}\right\},\qquad \left.\begin{aligned} \tilde{U}_{jR}^{\pm}&=|\tilde{U}_{jR}^{\pm}|\cdot e^{i\theta_{jR}^{u\pm}(z)} \\ \tilde{W}_{jR}^{\pm}&=|\tilde{W}_{jR}^{\pm}|\cdot e^{i\theta_{jR}^{w\pm}(z)} \end{aligned}\right\}, \tag{20d}$$

$$\left.\begin{aligned} \tilde{U}_{jR}^{+}&=U_{jR}^{+}+U_{jR}^{\mathrm{in}}\ , & \tilde{U}_{jR}^{-}&=U_{jR}^{-} \\ \tilde{W}_{jR}^{+}&=W_{jR}^{+}+W_{jR}^{\mathrm{in}}\ , & \tilde{W}_{jR}^{-}&=W_{jR}^{-} \end{aligned}\right\}, \tag{20e}$$

where $\{U_{jR}^{\pm}, W_{jR}^{\pm}\}$ $(j=1, 2)$ are given in (16b), (16c) and (16d).

Let us next consider the energy flux over one cycle in time of the waves scattered into the semi-infinite elastic body. The path c of the integration is given by θ which varies from 0 to π at $r=\infty$ and the stresses $\{X_c, Z_c\}$ in (18a) are given by (3) with substitution of suffix 2 for 1. The displacement $\{u_c, w_c\}$ is given by Re $\{We^{i\sigma t}, Ue^{i\sigma t}\}$ with $\{U, W\}$ in (17a).

Using (18a) with the help of the above-mentioned stresses and displacements, the energy of the body waves scattered into the semi-infinite elastic body E_{sc} becomes

$$E_{sc}=E_{sc}^{p}+E_{sc}^{s} , \tag{21a}$$

$$E_{sc}^{q}=\int_0^{\pi}\delta E_{sc}^{q}\,d\bar{\theta} \quad (q=p, s) \tag{21b}$$

$$\left.\begin{aligned}\delta E_{sc}^{p}&=(\lambda_2+2\mu_2)h_2^4\pi|\tilde{W}(\bar{\theta})|^2 ,\\ \delta E_{sc}^{s}&=\mu_2 k_2^4\pi|\tilde{U}(\bar{\theta})|^2 ,\end{aligned}\right\} \tag{21c}$$

where E_{sc}^{p} or E_{sc}^{s} indicates the energy flux due to P or S waves scattered into the elastic half space.

Let $\tilde{E}_{R}^{\mathrm{tr}}$, $\tilde{E}_{R}^{\mathrm{re}}$, $\tilde{E}_{jR}^{\mathrm{tr}}$, $\tilde{E}_{jR}^{\mathrm{re}}$ $(j=1, 2)$, $\tilde{E}_{sc}^{p}$, $\tilde{E}_{sc}^{s}$ and $\tilde{E}_{sc}$ be the energy fluxes normalized by the energy flux E_{R}^{in} of the incident Rayleigh waves. These normalized forms are expressed as

$$\tilde{E}_{R}^{\mathrm{tr}}=\tilde{E}_{1R}^{\mathrm{tr}}+\tilde{E}_{2R}^{\mathrm{tr}} , \qquad \tilde{E}_{R}^{\mathrm{re}}=\tilde{E}_{1R}^{\mathrm{re}}+\tilde{E}_{2R}^{\mathrm{re}} , \tag{22a}$$

$$\tilde{E}_{jR}^{\mathrm{tr}}=E_{jR}^{\mathrm{tr}}/E_{R}^{\mathrm{in}} , \qquad \tilde{E}_{jR}^{\mathrm{re}}=E_{jR}^{\mathrm{re}}/E_{R}^{\mathrm{in}} , \quad (j=1, 2) , \tag{22b}$$

$$\tilde{E}_{sc}=E_{sc}/E_{R}^{\mathrm{in}} , \qquad \tilde{E}_{sc}^{q}=E_{sc}^{q}/E_{R}^{\mathrm{in}} ,$$

and

$$\delta\tilde{E}_{sc}^{q}=\delta E_{sc}^{q}/E_{R}^{\mathrm{in}} \quad (q=p, s) . \tag{22c}$$

The conservation of energy is then expressed by

$$\tilde{E}_{\mathrm{total}}=(\tilde{E}_{R}^{\mathrm{tr}}+\tilde{E}_{R}^{\mathrm{re}})+\tilde{E}_{sc}^{p}+\tilde{E}_{sc}^{s}=1 , \tag{23}$$

where $\tilde{E}_{\mathrm{total}}$ is the normalized total energy. This equation will be used later in the evaluation of accuracy.

2.10 Leaky modes

In the study concerning the scattering of the edge waves in the ocean (paper I, 1976 b) we have already found the importance of the leaky mode of the edge waves, which are analogous to Love waves in the elastic medium. It is then found that the existence of leaky mode of the edge waves leads to the decrease of the transmitivity of the amplitude of the edge waves and the increase of the energy of the scattered waves into the ocean.

In this study concerning the scattering of Rayleigh waves we will find the similar results due to the existence of the leaky mode of P and S waves. First of all the simple theory of the leaky modes of P and S waves will be developed here.

The well-known type of Rayleigh waves is a trapped mode with the exponential part toward the inside of the medium. Meanwhile, if we assume a wave which has a component expressed as $\sin(\xi z+\eta)$ toward the inside of the medium, where ξ is a wave number and η the phase lag (arbitrary constant), there exists a kind of wave satisfying the boundary (surface and interface) conditions. Such a mode of waves is here named *leaky mode* after SNODGRASS *et al.*, (1962).

In the model with a *plane* free surface, the possibility of the existence of a stable leaky mode is very rare. Meanwhile, in the model with an *irregular* free surface, such a leaky mode is considered to play a very important role upon the transient waves scattered by the irregularity. This supposition will be found to be true in the discussion of energy partition in later sections.

Simple theory for P and S waves on leaky mode are, respectively, given here for the convenience of the discussion in later sections.

To begin with, consider first the case of P waves. Assume P waves expressed as

$$\left.\begin{aligned}\phi_1&=A_1\sin h_1z+B_1\cos h_1z\ ,\\ \phi_2&=A_2\cos\{h_2(z-H)\}+B_2\sin\{h_2(z-H)\}\ .\end{aligned}\right\}\tag{24a}$$

Substitution (24a) into (1b) yields

$$w_1=A_1h_1\cos h_1z-B_1h_1\sin h_1z\ ,\tag{24b}$$

$$w_2=-A_2h_2\sin\{h_2(z-H)\}+B_2h_2\cos\{h_2(z-H)\}\ .\tag{24c}$$

As known from the above expression, the displacement for P waves is normal to the free surface. By use of the conditions (2a) for $-\infty<X<\infty$, at the surface, the expression (24b) is reduced to

$$w_1=A_1h_1\cos h_1z\ .\tag{24b'}$$

Using the condition (4), continuity of displacement at the interface, and the expressions (24c) and (24b'), we have

$$A_1=B_2h_2/(h_1\cos h_1H)\ .\tag{24d}$$

Using the condition (2b), continuity of the stress, and (24c) and (24b'), we have

$$A_2=h_1^2A_1(\lambda_1+2\mu_1)\sin h_1H/(h_2^2(\lambda_2+2\mu_2))\ .$$

By use of (24d) the above expression becomes

$$A_2=B_2h_1(\lambda_1+2\mu_1)\sin h_1H/(h_2(\lambda_2+2\mu_2)\cos h_1H)\ . \tag{24e}$$

By substituting (24e) into (24c), the expression for w_2 becomes

$$\begin{aligned} w_2=&B_2h_2\cos(h_2(H-z))\\ &+B_2h_1lm_1\sin(h_1H)\sin(h_2(H-z))/(lm_2\cos(h_1H))\ , \end{aligned} \tag{24f}$$

with

$$lm_j=\lambda_j+2\mu_j\quad(j=1,\ 2)\ .$$

The expressions (24b′) with (24d) and (24f) are the final ones for the leaky mode of P waves.

Likewise, in the case of S waves we can obtain similar expressions. Then displacement component u is only horizontal. Assume S waves expressed as

$$\left.\begin{aligned} \psi_1&=C_1\sin k_1z+D_1\cos k_1z\ .\\ \psi_2&=C_2\cos\{k_2(z-H)\}+D_2\sin\{k_2(z-H)\}\ . \end{aligned}\right\} \tag{25a}$$

In a manner similar to the case of P waves, we have the expressions for the leaky mode of S waves by using the conditions at the surface and the interface,

$$u_1=k_1C_1\cos(k_1z) \tag{25b}$$

with

$$C_1=k_2D_2/(k_1\cos(k_1H)) \tag{25c}$$

in the upper layer and, in the substratum,

$$\begin{aligned} u_2=&D_2k_2\cos(k_2(H-z))\\ &+D_2k_1(\mu_1/\mu_2)\sin(k_1H)\sin(k_2(H-z))/\cos(k_1H)\ , \end{aligned} \tag{25d}$$

As readily found from (24b′) with (24d) and (25b) with (25c), the amplitudes in the upper layer are in resonance, when h_1H or $k_1H=(2n+1)\pi/2$ (n: integer), by making the denominator-cosine zero.

2.11 Accuracy of the theory

Following the procedure mentioned in the foregoing sections, numerical computation was carried out. The accuracy of the computation is as follows. If the number of the divisions at $\{|x|\leqq B,\ z=0\}$, i.e., M is 8 in the range of kB from 0 to 3.5, the error of the total energy $\sim|E_{\text{total}}-1|$ is suppressed to below 0.001. According to the results of the numerical computation, the accuracy of each energy flux $\tilde{E}^{\text{tr}}_{jR}$, $\tilde{E}^{\text{re}}_{jR}$ ($j=1,\ 2$), $\tilde{E}^{p}_{sc}$, $\tilde{E}^{s}_{sc}$ is of an order the same as that of the total energy.

3. Case of the Discontinuity of P wave velocity

In this section the following specified ratios of Lame's parameters

and density are used.

(i) $\lambda_1/\mu_1=1$, $\lambda_2/\mu_2=0.2$, $\mu_2/\mu_1=1$, $\rho_2/\rho_1=1$, $B/H=1$.

(ii) $\lambda_1/\mu_1=1$, $\lambda_2/\mu_2=20$, $\mu_2/\mu_1=1$, $\rho_2/\rho_1=1$, $B/H=1$.

That is to say, influence of the discontinuity of P wave velocity is discussed.

Let V_{pj} and V_{sj} $(j=1, 2)$ be the velocities of P and S waves in the domain D_j, i.e., the upper layer and the underlying half elastic space, respectively. These notations will be followed in the subsequent sections. The above two cases correspond to

(i) $V_{p2}/V_{p1}=0.85635$, $V_{s1}=V_{s2}$.

(ii) $V_{p2}/V_{p1}=2.70801$, $V_{s1}=V_{s2}$.

3.1 Energy fluxes of the transmitted and reflected Rayleigh waves

Energy fluxes of the transmitted ($\tilde{E}_{jR}^{tr}$) and reflected ($\tilde{E}_{jR}^{re}$) Rayleigh waves are computed for the two cases (i) and (ii) in the preface of this section. Variations of the results are given in Fig. 2 a. This figure reveals the following features.

The change of two curves for the change of Lame's parameters λ_2/μ_2 from 0.2 to 20 is very small.

The variation of the curve versus k_1H (abscissa) is very similar to

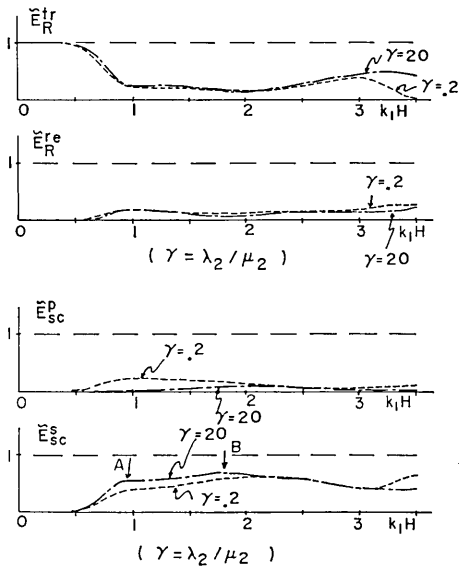

Fig. 2 a. Variations of energy partitions $\tilde{E}_R^{tr}$, $\tilde{E}_R^{re}$, $\tilde{E}_{cs}^{p}$ and $\tilde{E}_{sc}^{s}$ versus k_1H for the change of λ_2/μ_2 from 0.2 to 20 with constant $\lambda_1/\mu_1=\mu_2/\mu_1=\rho_2/\rho_1=B/H=1$ (case of the discontinuity of P wave velocity).

that in the case without a superimposed layer (paper II; 1980 b). For the transmitted Rayleigh waves in Fig. 2 a (top graph), we can find the same three typical features as those found in paper II i.e., (1) depression of the curve due to S wave resonance (near $k_1H=1.0$) occurring in the semi-circular mountain, (2) upheaval of the curve due to Rayleigh wave resonance (near $k_1H=3.0$) appearing along the curved surface of the mountain and (3) depression of the curve due to the resonance of P waves ($k_1H=3.5$) which has a displacement component normal to the curved surface of the mountain.

The most significant variation (depression) occurs at situation A in Fig. 2a, where the above (1)-type resonance is generated in the mountain.

Near $K_1H=1.8$ in the bottom graph (indicated as B) the curve of the scattered body S waves is upheaved. Near this value of k_1H, we can expect the resonant standing P waves of leaky mode through both the mountain and the upper layer where the relation of the wave number of P waves is expressed as $h_1(H+L*B)\sim\pi/2$ (then $h_1H=1.03$) with $L\sim0.5$. The parameter L is a value smaller than implying the effect of the roundness of the mountain.

3.2 Directivity of the scattered body waves

Variations of the density of energy flux of the scattered body waves, $\delta\tilde{E}^q_{sc}$ ($q=p, s$) given by (22c), are shown in Figs. 2 b-1 to 2 b-7, where the ordinate and sbscissa indicate the energy density $\delta\tilde{E}^q_{sc}$ of the scattered $P(S)$ body waves and aximuth θ, respectively.

In order to clarify the general features of the scattered body waves, consider the variation in the case of $k_1H=3.0$ (Fig. 2 b-6). In this graph three typical features are found, which are indicated by the characters A, B and C. Some physical interpretations for them will be given.

It must be noted that the azimuth where feature A occurs is about $\pi/4$. In the previous paper (MOMOI, 1980 a) concerning the scattering of Rayleigh waves in the quarter space, paper II (MOMOI, 1980 b) and the paper (MOMOI, 1985) concerning the scattering of Rayleigh waves in three quarter-space, we found the *breathing zone* of the scattered S waves which runs in the direction of about $\theta=\pi/4$ with high energy. The zone is produced as the result of the energy interchange between the *undeveloped* Rayleigh waves and the scattered S body waves.

As with feature B this sharp concentration of energy is explained by the traveling reflection and refraction of the P waves to the scattered S body waves at the free surface and the interface, as illustrated in the graph just below Fig. 2 b-6.

As with feature C the symmetrical pattern of the high energy is

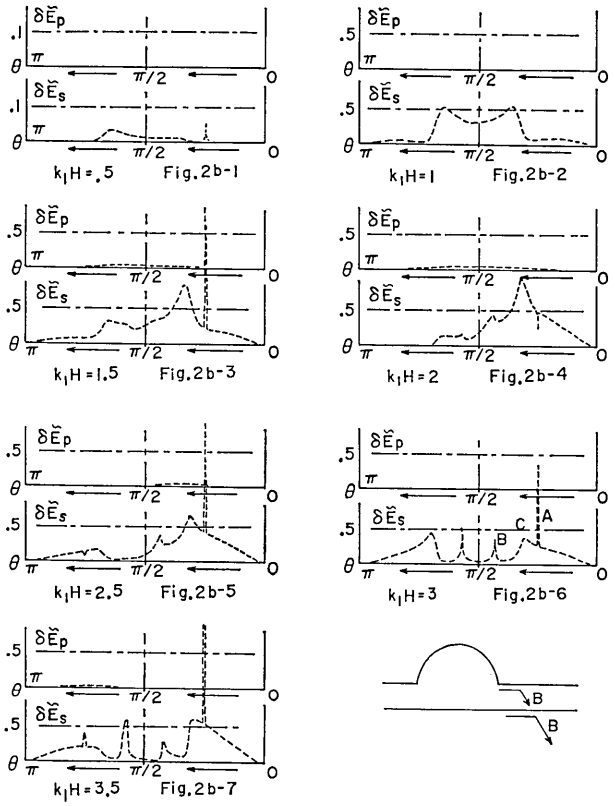

Fig. 2 b. Directivity of energy flux densities $\delta\tilde{E}_p$ and $\delta\tilde{E}_s$ of the scattered body waves for the change of k_1H from 0.5 (Fig. 2 b-1) to 3.5 (Fig. 2 b-7) as $\lambda_1/\mu_1=\mu_2/\mu_1=\rho_2/\rho_1=B/H=1$ and $\lambda_2/\mu_2=20$ (case of the discontinuity of P wave velocity).

considered to be caused by the waves reflected from the symmetrical curvature of the semi-circular mountain, since the top of the high energy is rather round.

Other than the other graphs, variations of the curves of energy in graphs 2 b-2 and 2 b-6 are symmetric with respect to $\theta=\pi/2$. This feature is attributed to the resonant standing S and Rayleigh waves occurring in the mountain near $k_1H=1.0$ and $k_1H=3.0$, respectively. Except for these two cases most of the scattered S body waves are directed toward the leeward quarter space ($\theta=0\sim\pi/2$) except for the case of the small k_1H (Fig. 2 b-1).

4. Case of the Discontinuity of Lame's constant μ

In this section the influence of the discontinuity of Lame's constant

μ is discussed by changing the parameter μ_2/μ_1 while other ones being invariant. The change of μ_2/μ_1 is accompanied by a change of velocities of both P and S waves.

4.1 Energy fluxes of the transmitted and reflected Rayleigh waves

In this section energy fluxes $\tilde{E}_R^{\mathrm{tr}}(\tilde{E}_R^{\mathrm{re}})$ of the transmitted (reflected) Rayleigh waves are computed for the specified values of Lame's constants,

$$\lambda_1/\mu_1=\lambda_2/\mu_2=\rho_2/\rho_1=B/H=1$$

and

$$\mu_2/\mu_1=3 \text{ (case i)}, \quad 4 \text{ (case ii)} \quad \text{and} \quad 5 \text{ (case iii)},$$

where these three cases correspond to the velocity ratios

$$V_{p2}/V_{p1}=V_{s2}/V_{s1}=1.73205,\ 2.00000 \quad \text{and} \quad 2.23607,$$

respectively.

Variations of the results are given in Figs. 3 a (case i), 3 b (case ii), and 3 c (case iii). The following features are exposed from these graphs.

As discussed in the foregoing section the striking depression of the curve $\tilde{E}_R^{\mathrm{tr}}$ (A in the top graph of each figure) due to S wave resonance in the mountain is found near $k_1H=1.0$ through the three case i, ii iii. The lost energy in energy $\tilde{E}_R^{\mathrm{tr}}$ appears in A in the curve $\tilde{E}_{sc}^{s}$ as the scattered S body waves (bottom in each graph).

The depression of the curve of the transmitted Rayleigh waves is seen near $k_1H=1.5(\sim\pi/2)$ (B in the top of each figure). Near this value of k_1H, the resonant standing S waves of the leaky mode are expected in the upper low-velocity layer, as stated in § 2.10. In the variation of the curve $\tilde{E}_{sc}^{s}$ for the scattered S waves (bottom in each figure), the curve is upheaved near here (shown as B).

Just before the appearance of the second mode of the Rayleigh waves, a particular partition of the energy occurs. These particular behaviors are seen near $k_1H=2.5$, 2.2 and 2.1 in Figs. 3 a, 3 b and 3 c, respectively. Through three cases the curves $\tilde{E}_{sc}^{s}$ for the scattered S waves (bottom graphs of Figs. 3 a, 3 b and 3 c) are upheaved near these values, as indicated as C there. It must be noted here that a little after these values of k_1H, the next second mode of the scattered Rayleigh waves appears. The depression of the curve $\tilde{E}_{sc}^{s}$, just after these values, is due to the occurrence of the subsequent second mode of the scattered Rayleigh waves.

A similar feature is also exposed in the studies of the L-shaped channel (MOMOI, 1974) and the closed L-shaped channel (MOMOI, 1976 a)

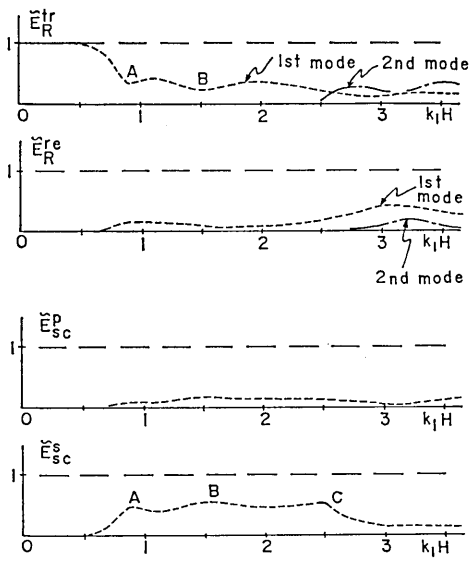

Fig. 3a. Variations of energy partitions $\tilde{E}_R^{tr}$, $\tilde{E}_R^{re}$, $\tilde{E}_{sc}^{p}$ and $\tilde{E}_{sc}^{s}$ versus k_1H as $\lambda_1/\mu_1=\lambda_2/\mu_2=\rho_2/\rho_1=B/H=1$ and $\mu_2/\mu_1=3$ (case of the discontinuity of P and S wave velocity).

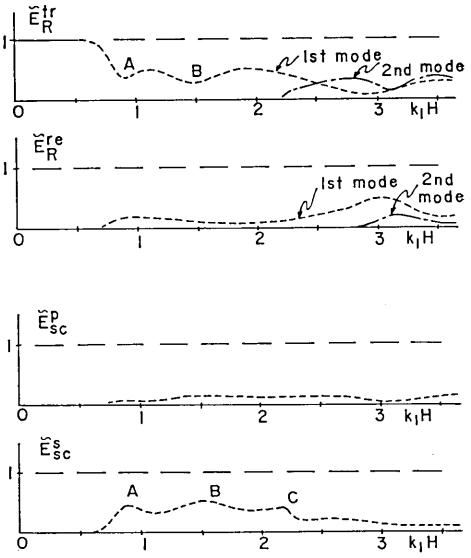

Fig. 3b. Variations of energy partitions $\tilde{E}_R^{tr}$, $\tilde{E}_R^{re}$, $\tilde{E}_{sc}^{p}$ and $\tilde{E}_{sc}^{s}$ versus k_1H as $\lambda_1/\mu_1=\lambda_2/\mu_2=\rho_2/\rho_1=B/H=1$ and $\mu_2/\mu_1=4$ (case of the discontinuity of P and S wave velocity).

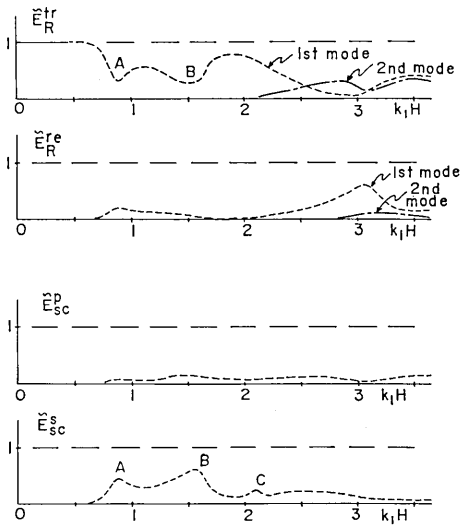

Fig. 3c. Variations of energy partitions $\tilde{E}_R^{tr}$, $\tilde{E}_R^{re}$, $\tilde{E}_{sc}^{p}$ and $\tilde{E}_{sc}^{s}$ versus k_1H as $\lambda_1/\mu_1=\lambda_2/\mu_2=\rho_2/\rho_1=B/H=1$ and $\mu_2/\mu_1=5$ (case of the discontinuity of P and S wave velocity).

for the incidence of periodic water waves. In these works we found that, just before the appearance of the advancing wave of the m-th higher mode, the energy of the preceding $(m-1)$-th lower mode is increased by the supply with the energy from the higher m-th mode which is trapped near the corner due to its evanescent mode.

In the present case in the range before the generation of the new higher mode, the scattered energy is confined in the upper layer as the *potential* Rayleigh waves. The potential Rayleigh waves cannot transmit along the surface as the trapped mode of Rayleigh waves, but the energy is scattered away toward the semi-infinite half body, papticularly along the interface on the positive side of x (see Fig. 4 d-5 in § 4.2).

Another interesting feature is that, in the second graphs associated with $\tilde{E}_R^{\mathrm{re}}$ of Figs. 3 a, 3 b and 3 c, the curve of the reflected Rayleigh waves is upheaved near $k_1H=3.0$. Unfortunately, the physical meaning of the phenomenon is not clear.

4.2 Directivity of the scattered body waves

In this section the variations of the directivity of the scattered body waves are discussed for the following specified values of Lame's constants.

The used ratios of Lame's parameters and density are

$$\lambda_1/\mu_1=\lambda_2/\mu_2=\rho_2/\rho_1=B/H=1$$

and

$$\mu_2/\mu_1=0.8 \text{ (case i)}, \quad 1 \text{ (case ii)}, \quad 2 \text{ (case iii)},$$
$$3 \text{ (case iv)}, \quad 4 \text{ (case v)} \quad \text{and} \quad 5 \text{ (case vi)},$$

where there exist the relations $(j=p, s)$

$$V_{p2}/V_{p1}=V_{s2}/V_{s1}$$
$$=0.89443,\ 1.00000,\ 1.41421,\ 1.73205,\ 2.00000 \quad \text{and} \quad 2.23607$$

for cases (i), (ii), (iii), (iv), (v) and (vi).

Variations of the results are given in Figs. 4 a (case i), 4 b (case ii), 4 c (case iii), 4 d (case iv), 4 e (case v) and 4 f (case vi), each of which has seven graphs, respectively.

These seven graphs show the variations for specified values of $k_1H=0.5$ (no. 1), 1.0 (no. 2), 1.5 (no. 3), 2.0 (no. 4), 2.5 (no. 5), 3.0 (no. 6) and 3.5 (no. 7), respectively.

Through Figs. 4 c-4 f (cases $V_{j1}<V_{j2}$) the same interesting characteristic is seen. In graphs from no. 2 (case $k_1H=1$) up to no. 4 (case $k_1H=2$) the location, in azimuth, of two sharp upheavals moves gradually in the direction $\theta=0$, i.e., toward the interface, as indicated as

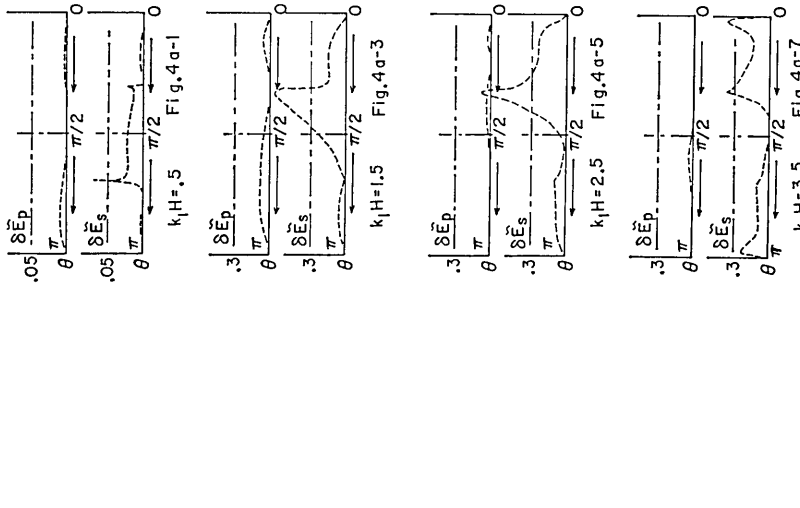

Fig. 4 a. Directivity of energy flux densities $\delta\tilde{E}_p$ and $\delta\tilde{E}_s$ of the scattered body waves for the change of k_1H from 0.5 (Fig. 4 a-1) to 3.5 (Fig. 4 a-7) as $\lambda_1/\mu_1=\lambda_2/\mu_2=\rho_2/\rho_1=B/H=1$ and $\mu_2/\mu_1=0.8$ (case of the discontinuity of P and S wave velocity).

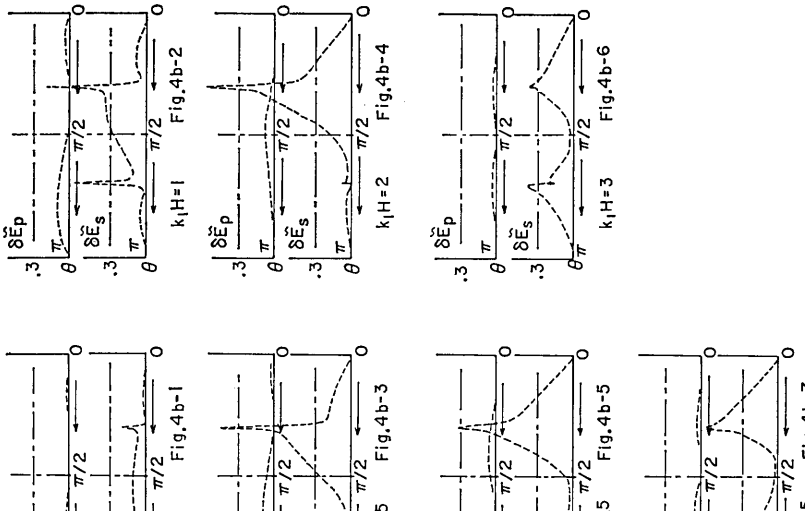

Fig. 4 b. Directivity of energy flux densities $\delta\tilde{E}_p$ and $\delta\tilde{E}_s$ of the scattered body waves for the change of k_1H from 0.5 (Fig. 4 b-1) to 3.5 (Fig. 4 b-7) as $\lambda_1/\mu_1=\lambda_2/\mu_2=\rho_2/\rho_1=B/H=1$ and $\mu_2/\mu_1=1$ (case of the discontinuity of P and S wave velocity).

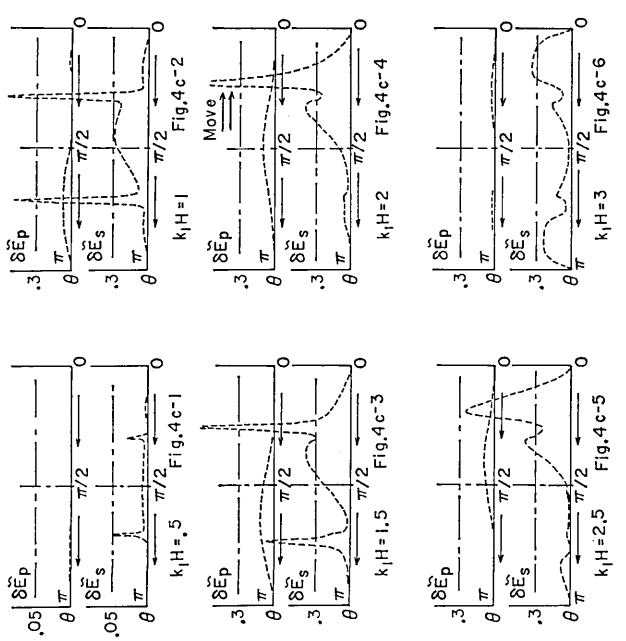

Fig. 4c. Directivity of energy flux densities $\delta\tilde{E}_p$ and $\delta\tilde{E}_s$ of the scattered body waves for the change of k_1H from 0.5 (Fig. 4c-1) to 3.5 (Fig. 4c-7) as $\lambda_1/\mu_1=\lambda_2/\mu_2=\rho_2/\rho_1=B/H=1$ and $\mu_2/\mu_1=2$ (case of the discontinuity of P and S wave velocity).

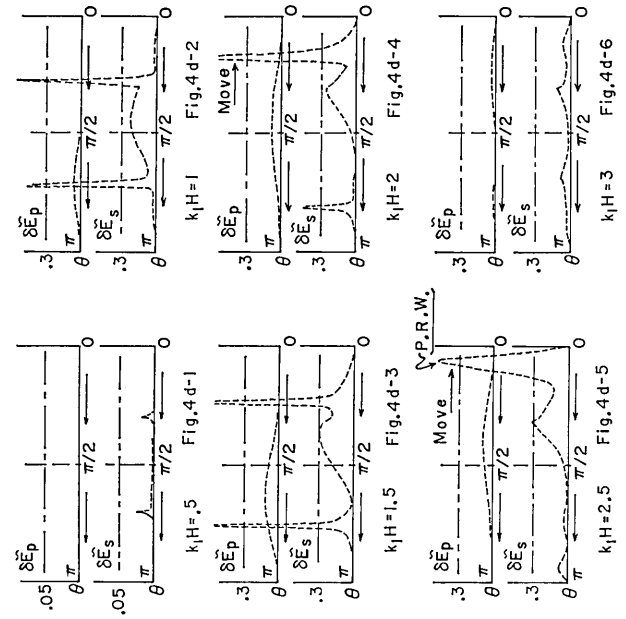

Fig. 4d. Directivity of energy flux densities $\delta\tilde{E}_p$ and $\delta\tilde{E}_s$ of the scattered body waves for the change of k_1H from 0.5 (Fig. 4d-1) to 3.5 (Fig. 4d-7) as $\lambda_1/\mu_1=\lambda_2/\mu_2=\rho_2/\rho_1=B/H=1$ and $\mu_2/\mu_1=3$ (case of the discontinuity of P and S wave velocity).

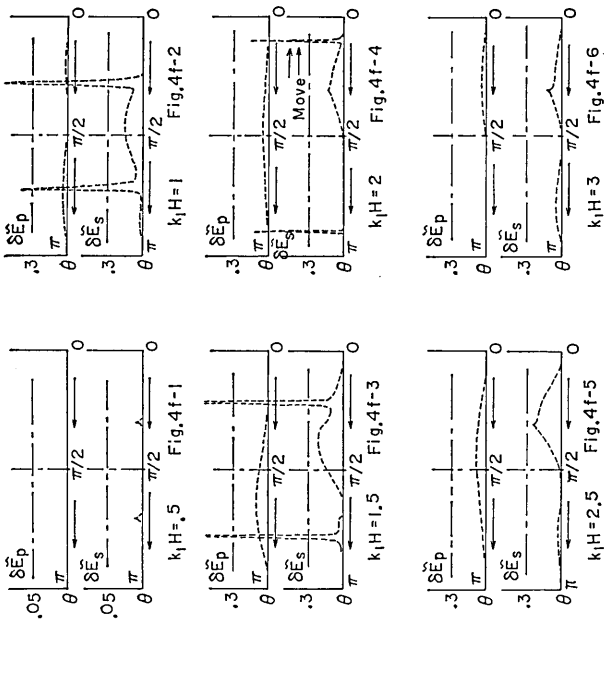

Fig. 4 e. Directivity of energy flux densities $\delta\tilde{E}_p$ and $\delta\tilde{E}_s$ of the scattered body waves for the change of k_1H from 0.5 (Fig. 4 e-1) to 3.5 (Fig. 4 e-7) as $\lambda_1/\mu_1=\lambda_2/\mu_2=\rho_2/\rho_1=B/H=1$ and $\mu_2/\mu_1=4$ (case of the discontinuity of P and S wave velocity).

Fig. 4 f. Directivity of energy flux densities $\delta\tilde{E}_p$ and $\delta\tilde{E}_s$ of the scattered body waves for the change of k_1H from 0.5 (Fig. 4 f-1) to 3.5 (Fig. 4 f-7) as $\lambda_1/\mu_1=\lambda_2/\mu_2=\rho_2/\rho_1=B/H=1$ and $\mu_2/\mu_1=5$ (case of the discontinuity of P and S wave velocity).

"Move" in the graph no. 4. The extent of the movement becomes more remarkable with the increase of μ_2/μ_1.

As mentioned in the previous section, just before the succeding higher mode of Rayleigh waves appears, the scattered S body waves run along the interface toward the leeward side. "P.R.W." in the graph indicates *Potential Rayleigh Waves* (see Fig. 4 d-5).

Two sharp upheavals also appear even though there is no layer (see Fig. 4 b, case $\mu_2/\mu_1=1$). But there exists a outstanding difference between the two cases with and without a layer. That is to say, the location of sharp upheavals in the case without a layer (Fig. 4 b) never moves for the change of the variable k_1H.

5. Case of the discontinuity of density

In this section influence of the discontinuity of the density on the partition of the energy is discussed.

5.1 Energy flux of the transmitted Rayleigh waves

In this section energy fluxes of the transmitted Rayleigh waves are computed for the following specified values of Lame's constants and densities.

$$\lambda_1/\mu_1=\lambda_2/\mu_2=\mu_2/\mu_1=B/H=1$$

and

$$\rho_2/\rho_1=0.5,\ 1.1,\ 1.2,\ 1.3 \quad \text{and} \quad 1.4$$

(cases i, ii, iii, iv and v, respectively),

where the ratios of the velocities are

$$V_{p2}/V_{p1}=V_{s2}/V_{s1}$$
$$=1.41421,\ 0.95346,\ 0.91287,\ 0.87706 \quad \text{and} \quad 0.84515,$$

respectively.

Variations of the result are given in Figs. 5 a-1, -2, -3, -4 and -5 (cases i, ii, iii, iv and v, respectively). In Figs. 5 a-4 and 5 a-5, the curves showing the variation terminate around $k_1H=2.8$ and 2.0, respectively. The terminations are due to the vanishing of Rayleigh waves there. These graphs reveal the very interesting feature that the transmissibility of the Rayleigh waves through the mountain becomes better with the increase of the ratio of the density ρ_2/ρ_1. In the practical case of the earth, the density increases with the depth and, therefore, this structure of the earth helps better the transmissibility of the Rayleigh waves.

In order to examine the physical meaning of the above feature,

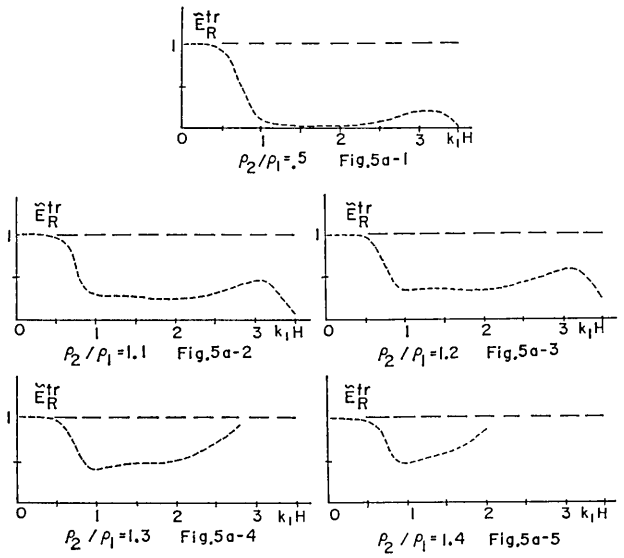

Fig. 5a. Variations of the energy flux $\tilde{E}_R^{tr}$ of the transmitted Rayleigh waves for the change of ρ_2/ρ_1 from 0.5 (Fig. 5a-1) to 1.4 (Fig. 5a-5) as $\lambda_1/\mu_1=\lambda_2/\mu_2=\mu_2/\mu_1=B/H=1$ (case of the discontinuity of the density).

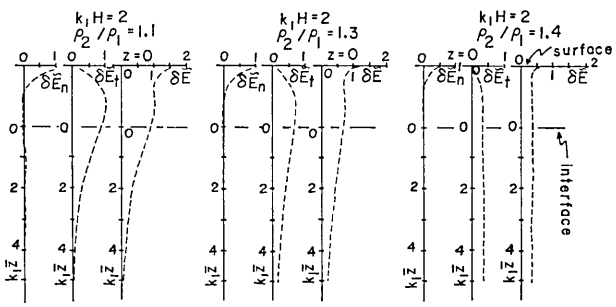

Fig. 5b. Transition of energy profile of Rayleigh waves for the change ρ_2/ρ_1 from 1.1 (leftmost) to 1.4 (rightmost) as $\lambda_1/\mu_1=\lambda_2/\mu_2=\mu_2/\mu_1=B/H=1$. Absciasa: density of energy flux; Ordinate: k_1z as $\bar{z}=z-H$ (vertically downward). $\delta\tilde{E}_n$ and $\delta\tilde{E}_t$: energy flux densities due to the stresses normal and tangential to the plane perpendicular to the x-axis. $\delta\tilde{E}$: sum of $\delta\tilde{E}_n$ and $\delta\tilde{E}_t$.

the energy profiles of the energy flux of Rayleigh waves versus depth (z-axis) are given in Fig. 5b, where only the three cases of $\rho_2/\rho_1=1.1$, 1.3 and 1.4 are given. This figure shows that, for small $\rho_2/\rho_1(=1.1)$, the energy of the waves is concentrated near the free surface while, for large $\rho_2/\rho_1(=1.4)$, the energy profile is flat. The concentration of the energy flux near the surface (case $\rho_2/\rho_1=1.1$) results in the larger scattering of waves due to the surface irregularity. These patterns

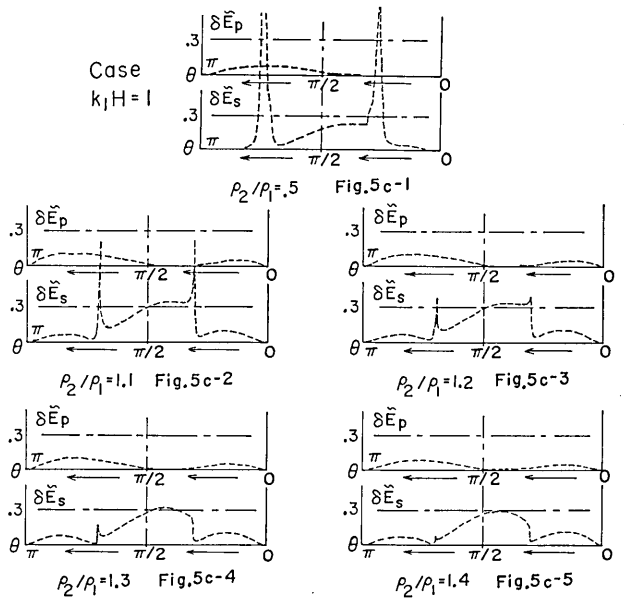

Fig. 5c. Directivity of energy flux densities $\delta\tilde{E}_p$ and $\delta\tilde{E}_s$ of the scattered body waves for the change of ρ_2/ρ_1 from 0.5 (Fig. 5c-1) to 1.4 (Fig. 5c-5) as $k_1H=1$ and $\lambda_1/\mu_1=\lambda_2/\mu_2=\mu_2/\mu_1=B/H=1$ (case of the discontinuity of the density).

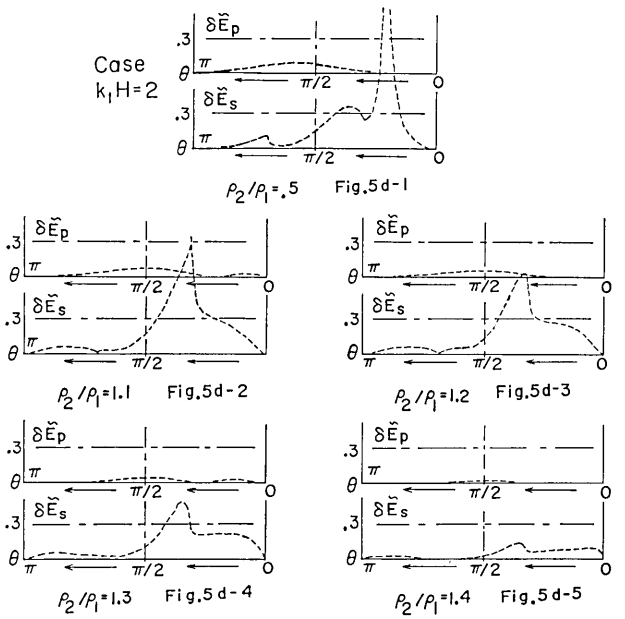

Fig. 5d. Directivity of energy flux densities $\delta\tilde{E}_p$ and $\delta\tilde{E}_s$ of the scattered body waves for the change of ρ_2/ρ_1 from 0.5 (Fig. 5d-1) to 1.4 (Fig. 5d-5) and $k_1H=2$ as $\lambda_1/\mu_1=\lambda_2/\mu_2=\mu_2/\mu_1=B/H=1$ (case of the discontinuity of the density).

of the energy profile yield better transmissibility of Rayleigh waves for larger ρ_2/ρ_1.

5.2 Directivity of the scattered waves

In Figs. 5 c and 5 d (nos. 1, 2, 3, 4, 5), the variation of the energy density versus the azimuth is given for the specified value of $k_1H=1.0$ and 2.0, respectively. The used values of λ_1/μ_1, λ_2/μ_2, μ_2/μ_1 and ρ_2/ρ_1 are the same as those given in the previous section (see the head of § 5.1).

These figures show that the energy of the scattered body waves decreases in amount with the increase of ρ_2/ρ_1. The sharpness of the upheaval of the curve due to the traveling reflection gradually disappears with the increase of ρ_2/ρ_1.

6. Dependence of energy partition on the ratio H/B in the case of discontinuity of P wave velocity

In the above sub-title B and H stand for half a width of the semi-circular mountain and the thickness of the layer. In this and the next sections the discussions will be made about the effect of the change of the thickness of the upper layer upon the partition of the energy of the scattered waves.

To begin with, in this section the case of discontinuity of P wave velocity is considered. The used values are as follows:

$$B/H=0.5 \quad \text{and} \quad 1.0$$

for constant $\lambda_1/\mu_1=1$, $\lambda_2/\mu_2=20$, $\mu_2/\mu_1=1$ and $\rho_2/\rho_1=1$.

6.1 Energy of the transmitted Rayleigh waves

Variation of the energy $\tilde{E}_R^{tr}$ of the transmitted Rayleign waves versus k_1B is given in Fig. 6 a for the two cases $B/H=0.5$ (left) and 1.0 (right). The changing patterns of the curves for the two cases are very similar except for one point. In the case of Fig. 6 a-2 (on the right side) the curve is depressed near the value of $k_1B=2.0$. The corresponding value of $h_1(B+L)$ associated with P waves ($h_1B\sim1.1$) is then about $\pi/2$, where L is assumed nearly $B/2$ by taking the roundness of the mountain into account. That is to say, the resonance of standing P waves of the leaky mode is expected through the mountain and the upper layer.

6.2 Energy of the scattered body waves

The variation of the energy $\tilde{E}_{sc}^{p}$ of the scattered P body waves is given in Figs. 6 b (nos. 1 and 2). In the curves of these graphs, two

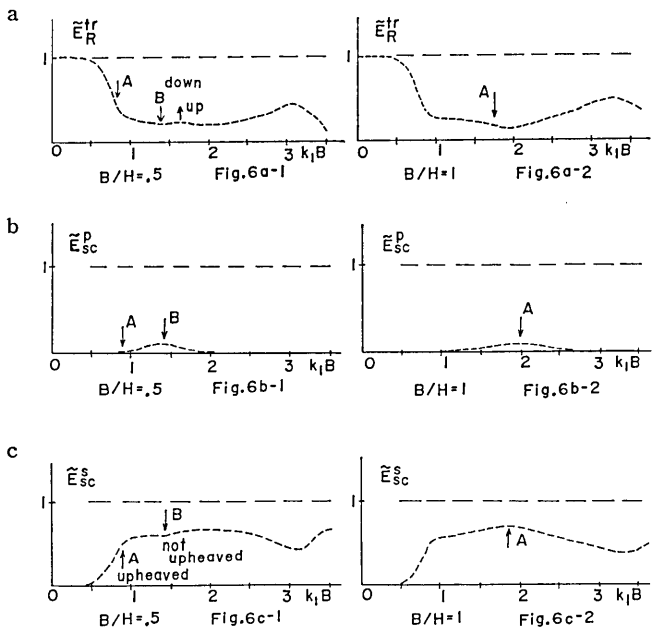

Figs. 6 a (top), 6 b (second) and 6 c (bottom). Variations of energy flux $\tilde{E}_R^{tr}$ (top), $\tilde{E}_{sc}^{p}$ (second) and $\tilde{E}_{sc}^{s}$ (bottom) for the change of the thickness (H) of the superimposed layer from $B/H=0.5$ (left) to 1 (right) as constant $\lambda_1/\mu_1=\mu_2/\mu_1=\rho_2/\rho_1=1$ and $\lambda_2/\mu_2=20$.

upheavals B (in the case no. 1) and A (in the case no. 2), are found. B is produced by the leaky mode of the resonant standing P waves ($h_1B=1.6$, i.e., about $\pi/2$ at $k_1B=1.4$) while A is caused by that through the mountain and the upper layer ($h_1(B+L)\sim\pi/2$).

The variation of the energy $\tilde{E}_{sc}^{s}$ of scattered S body waves is also given in Figs. 6 c (nos. 1 and 2). Inspection of these graphs reveals two interesting phenomena with reverse features. First, the occurrence of the leaky mode of the resonant standing P waves through both the mountain and the upper layer results in the increase of the scattered S body waves, as indicated by A-part (upheaved) in the two graphs. Second, the occurrence of the leaky mode of the resonant standing P waves only in the upper layer yields the reverse result, i.e., the depression of the curve, as indicated as "not upheaved" in B-part. The two reverse effects of the standing P waves is explained as follows. In the case of the resonant standing P waves through both the mountain and the upper layer (case A), P waves near the mountain are more converted to S waves due to the circularity of the mountain than in the case of the standing P waves only in the upper layer (then straight boundary, case B).

7. Dependence of energy partition on the ratio B/H in the case of discontinuity of Lame's constant μ

In this section we will discuss the effect of the change of the thickness of the upper layer upon the partition of energy of the scattered waves in the case of discontinuity of Lame's constant μ. The used values are

$$B/H=0.5,\ 1.0,\ 2.0 \quad \text{and} \quad 5.0$$

for constant $\lambda_1/\mu_1=\lambda_2/\mu_2=\rho_2/\rho_1=1$ and $\mu_2/\mu_1=3.0$.

7.1 Energy of the transmitted Rayleigh waves

The variation of the energy of the transmitted Rayleigh waves versus k_1B is given in Fig. 7 a for $B/H=0.5$ (no. 1), 1.0 (no. 2), 2.0 (no. 3) and 5.0 (no. 4), where the numbers in the parentheses refer to Fig. 7 a-# (#=1, 2, 3, 4). These graphs reveal the typical effect of the change of the thickness of the upper layer.

Throughout the graphs of Fig. 7 a, the sharp depression (indicated as A) of the curve is found near $k_1B=1.0$, where resonant standing S waves appear in the semi-circular mountain, as already discussed.

Near $k_1B=1.0$ in graphs nos. 2, 3 and 4, in addition to the resonant standing S waves in the mountain, the resonant standing S waves of leaky mode through both the mountain and upper layer are expected at the situation indicated as C_1 very close to A, since $k_1(B+H)L\sim\pi/2$, where L is the factor with some value less than 1.0 indicating the effect of the roundness of the mountain. The modification of the above expression leads to

$$k_1B\sim(\pi/2)/\{(1+H/B)L\}\ .$$

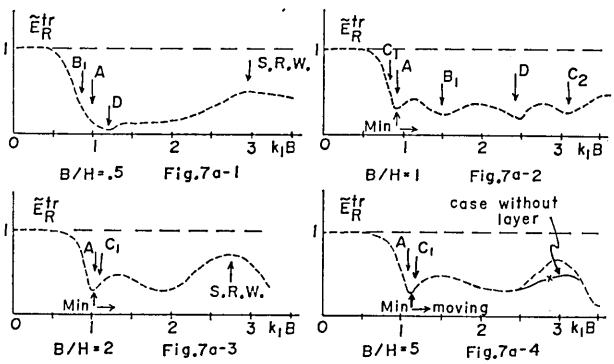

Figs. 7 a. Variations of energy flux $\tilde{E}_R^{tr}$ of the transmitted Rayleigh waves for the change of the thickness (H) of the superimposed layer from $B/H=0.5$ (Fig. 7 a-1) to 5 (Fig. 7 a-4) as constant $\lambda_1/\mu_1=\lambda_2/\mu_2=\rho_2/\rho_1=1$ and $\mu_2/\mu_1=3$.

From this expression the value of k_1B, though there exists some ambiguity in the evaluation of L, is found to increase with $B/H=1.0$, 2.0 and 5.0 or with the decrease of H/B. This feature reflects the fact that the minimum part C_1 of the curve is in a tendency of shifting-up in the direction of larger k_1B with the increase of B/H.

In Figs. 7 a (nos. 1 and 2) the depression (indicated as B_1) of the curve occurs near $k_1B=0.9$ (no. 1) and 1.5 (no. 2). The corresponding value of k_1H is $\pi/2$, whereby the resonant standing S waves of leaky mode are expected in the upper layer. Near $k_1B=3.0$ in Fig. 7 a-2 (indicated as C_2) we can find also the depression due to the resonant standing S waves of the leaky mode through both the mountain and the upper layer.

In Figs. 7 a (nos. 1 and 2) the depressions of the curve are also found at the parts indicated as D. The corresponding values of k_1B at D are the values just after that the second mode of Rayleigh waves is produced. Meanwhile, the reciprocal results of the above mentioned depressions appear, in a form of the elevation of the curve, at part D in Figs. 7 c (no. 1 and no. 2) associated with the scattered S body waves.

The standing Rayleigh waves are produced along the curved surface of the mountain near $k_1B=3.0$ and the generation of the standing Rayleigh waves enhances the transmissibility of the transmitted Rayleigh waves through the mountain (paper II). Meanwhile, in the case of Fig. 7 a-2, the resonant standing S waves (the second mode) of leaky mode occur near $k_1B=3.0$, through the mountain and the upper layer. It makes the transmissibility of Rayleigh waves decrease near there.

In Fig. 7 a-4 the curve of energy of the transmitted Rayleigh waves in the case without the upper layer is also inserted in solid line. By comparing two curves in the cases with and without a layer, the transmissibility of the waves is found much better in the case with a layer when the thickness of the layer is small (then B/H large). This is considered to be due to the generation of stronger standing Rayleigh waves along the curved surface of the mountain by the existence of the upper layer.

7.2 Energy of the scattered body waves

Variations of the energy fluxes, $\tilde{E}^p_{sc}$ and $\tilde{E}^s_{sc}$ of the scattered P and S body waves are given in Figs. 7 b and 7c for the change of B/H (nos. 1, 2, 3 and 4), respectively.

In Fig. 7 b associated with P waves the noticeable difference in the variation cannot be found for the change of B/H. Meanwhile, in the case of $\tilde{E}^s_{sc}$ associated with S waves the reciprocal parts of the energy at the depressed parts in the curve $\tilde{E}^{tr}_R$, associated with the

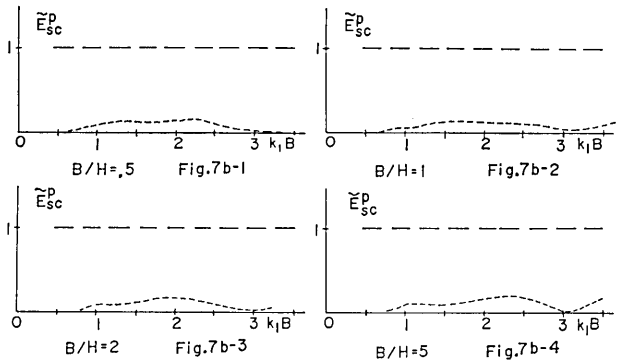

Figs. 7 b. Variations of energy flux $\tilde{E}^p_{sc}$ of the scattered P body waves for the change of the thickness (H) of the superimposed layer from $B/H=0.5$ (Fig. 7 b-1) to 5 (Fig. 7 b-4) as constant $\lambda_1/\mu_1=\lambda_2/\mu_2=\rho_2/\rho_1=1$ and $\mu_2/\mu_1=3$.

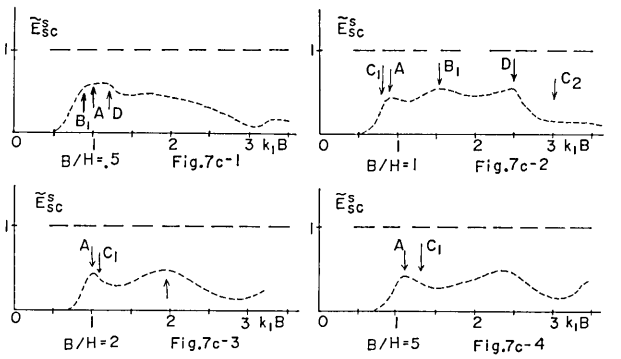

Figs. 7 c. Variations of energy flux $\tilde{E}^s_{sc}$ of the scattered S body waves for the change of the thickness (H) of the superimposed layer from $B/H=0.5$ (Fig. 7 c-1) to 5 (Fig. 7 c-4) as constant $\lambda_1/\mu_1=\lambda_2/\mu_2=\rho_2/\rho_1=1$ and $\mu_2/\mu_1=3$.

transmitted Rayleigh waves, appear as the upheaved curves at the parts A, B_1, C_1, and D in Fig. 7 c.

Conclusion

Obtained results are summarized here.

(1) The most important and interesting characteristic, among the facts exposed in this paper, is the effect of the resonant standing P and S waves of the leaky mode occurring in the upper layer or through both the upper layer and the mountain. The resonant standing waves of leaky mode are produced at the place

$$h_1H \quad \text{or} \quad k_1H=(2n+1)\pi/2 \quad (n=0, 1, 2, \cdots)$$

for P or S waves.

In general, the existence of the above mentioned standing waves makes the transmissibility of the transmitted Rayleigh waves decrease and the energy of the scattered body waves, particularly S body waves, increases.

(2) In the study (paper II, 1980 b) concerning the scattering of Rayleigh waves due to the semi-circular rough surface in the model without the upper layer, we found the characteristics that (a) the occurrences of the resonant standing S and P waves in the mountain, near $k_1B=1.0$ (for S) and 3.5 (for P), result in the abrupt decreases of the transmissibility of the transmitted Rayleigh waves through the mountain. (b) Meanwhile, near $k_1B=3.0$, the resonant standing Rayleigh waves along the curved surface causes the converse result, i.e., high transmissibility of the transmitted Rayleigh waves. Characteristic (b) is considered to be due to the confinement of the energy of the waves along the free surface.

Even in the case of the presence of the superimposed layer (present study), the same characteristics (a) and (b) mentioned above are found. In addition to these two, the presence of the upper layer causes the secondary undulations upon the change pattern of the energy partition in the case without the upper layer. The secondary undulations are induced by the leaky modes of P and S waves, such as described in paragraph (1) of this conclusion. Typical instances are elucidated in sections 3 to 7.

(3) Just before the appearance of the second mode of the scattered Rayleigh waves, the energy flux of the transmitted Rayleigh waves decreases and the decreased energy is converted into the scattered S body waves (C in the bottom graphs of Figs. 3 a, b, c and D in Figs. 7 a, c). The leading part of the energy of the scattered S body waves then runs along the interface on the leeward side of the mountain (P.R.W. in Fig. 4 d-5).

(4) In the case of the discontinuity of density (§ 5), where $\rho_2/\rho_1=$ 0.5, 1.1, 1.2, 1.3 and 1.4 with other parameters being invariant, it is found that the transmissibility of Rayleigh waves through the mountain becomes higher with the increase of the ratio of the density ρ_2/ρ_1. In the practical case of the earth the density ratio increases with the depth.

References

Brebbia, C. A., 1978, The Boundary Element Method for Engineers, Pentech Press, London.

Cisternas, A. and G. Jobert, 1977, Extension of matrix methods to structures with slightly irregular stratification, *J. Geophys.*, 43, 59-74.

Doornbos, D. J., 1978, On seismic wave scattering by a rough core-mantle boundary, *Geophys. J.*, 53, 643-662.

DRAKE, L. A., 1972, Rayleigh waves at a continental boundary by the finite element method, *Bull. Seismol. Soc. Am.*, **62**, 1259–1268.

EWING, W. M., W. S. Jardetzky and F. Press, 1957, Elastic Waves in Layered Media, McGraw-Hill, New York.

FUJII, K., Y. NAKAYAMA, K. IMAI and M. NAKANO, 1980a, Group of Rayleigh waves transmitted across a trench on the surface of elastic half-space (I), *Zisin (J. Seism. Soc. Japan)* **33**, 1–10.

FUJII, K., Y. NAKAYAMA and M. NAKANO, 1980b, Group of Raylengh waves transmitted across a trench on the surface of elastic half-space (II), *Zisin (J. Seism. Soc. Japan)* **33**, 11–22.

FUJII, K., T. TAKIMOTO and M. NAKANO, 1980c, An analysis of Rayleigh waves transmitted across a trench, *Technological Report of Kansai Univ.*, 221–231.

FUYUKI, M. and Y. MATSUMOTO, 1980, Finite difference analysis of Rayleigh wave scattering at a trench, *Bull. Seismol. Soc. Am.*, **70**, 2051–2069.

LAMB, M., 1904, On the propagation of tremos over the surface of an elastic solid, *Phil. Trans. Roy. Soc. London, Ser. A*, **203**, 1–42.

LYSMER, J. and L. A. DRAKE, 1971, The propagation of Love waves across nonhorizontally layered structures, *Bull. Seismol. Soc. Am.*, **61**, 1233–1252.

LYSMER, J. and L. A. DRAKE, 1972, A finite element method for seismology, in Methods in Computational Physics 11, Seismology, ed. B. Alder, S. Fernbach and B. A. Bolt, Ch. 6, Academic Press, New York.

MARTEL, L., M. MUNASINGHE and G. W. FARNELL, 1977, Transmission and reflection of Rayleigh wave through a step, *Bull. Seismol. Soc. Am.*, **67**, 1277–1290.

MOMOI, T., 1974, A long wave in an L-shaped channel, *J. Phys. Earch.* **22**, 395–414.

MOMOI, T., 1976a, Resonance in a closed L-shaped channel, *J. Phys. Earth.* **24**, 205–214.

MOMOI, T., 1976b, Scattering of long waves at the mouth of estuaries bordering on a continental shelf. *J. Phys. Earth.*, **24**, 1–25. (paper I)

MOMOI, T., 1980a, Scattering of Rayleigh waves in an elastic quarter space, *J. Phys. Earth*, **28**, 385–413.

MOMOI, T., 1980b, Scattering of the Rayleigh wave by a semi-circular rough surface, *J. Phys. Earth*, **28**, 497–519. (paper II)

MOMOI, T., 1981, Scattering of long waves at the mouth of estuaries bordering on a continental shelf. Part III. *J. Phys. Earth*, **29**, 187–200. (paper III)

MOMOI, T., 1982, Scattering of Rayleigh waves by a rectangular rough surface, *J. Phys. Earth*, **30**, 295–319. (paper IV)

MOMOI, T., 1985, Scattering of Rayleigh waves in an elastic three-quater space, *J. Phys. Earth*, **33**, 323–343.

SATÔ, Y., 1972, A numerical experiment on wave propagation in an elastic quarter space, *J. Phys. Earth*, **20**, 287–299.

SNODGRASS, F. E., W. H. MUNK and G. R. MILLER, 1962, Long period waves over California's continental borderland. Part I. Background spectra, *J. Mar. Res.*, **20**, 3–30.

SUTEAU, A. and L. MARTEL, 1980, Surface waves in structures with locally irregular boundaries, *Bull. Seismol. Soc. Am.*, **70**, 791–808.

WOODHOUSE, J. H., 1974, Surface waves in a laterally varying layered structure, *Geophys. J.*, **37**, 461–490.

ZAMA, S., 1981, Behavior of the elastic waves propagating through the irregular structures. I. Effects on the cliff by earthquake ground motion, *Bull. Earthq. Res. Inst., Tokyo Univ.*, **56**, 741–752.

成層半無限の弾性体上にある半円形の地形にもとづくレーリー波の散乱について

地震研究所　桃井高夫

(1) 本論文において得られた最も重要で興味ある特性は，P または S 波の振幅が媒質内部で三角関数 (sine, cosine) 的に変化する共鳴定常波 (leaky mode) が地表近くに発生したとき，地表にある半円形地形に突入したレーリー波によって起こされた散乱波群（透過および反射レーリー波，弾性体内部への散乱実体 P および S 波よりなる）へのエネルギーが下記のような異常な配分を受けることである．

一般に，上述の定常波の存在は透過レーリー波へのエネルギー配分を低下させ，弾性体内部への散乱実体 P および S 波へのエネルギー配分を増加させる．

(2) 前に，筆者 (1980 b) は層をもたない半無限弾性体の表面にある半円形の起伏によるレーリー波の散乱についての研究を行った．そのとき得られた結果は今回の研究でもやはり見いだされている．すなわち，(a) 半円形の山の部分に発生する共鳴定常 P または S 波は透過レーリー波の透過性を低下させ，(b) 半円形の山の部分に発生する定常レーリー波は透過レーリー波の透過性を逆に高める．

今回の研究では，地表面の近くに発生する leaky な定常 P, S 波の影響が上述の (a) (b) にもとづく散乱波のエネルギー配分の変化に更に上乗せするかたちで現れている．

(3) 透過レーリー波の第一のモードだけが存在する状態から第二のモードが発生する直前で透過レーリー波の総エネルギー（第一，第モードの和）は減少し，その減少したエネルギーは散乱実体 S 波として媒質内部に散乱される．そしてそのエネルギーは主に，上層と下層の境界面に沿って伝播する．

(4) 上下の層で媒質の密度に変化がある場合，下層の密度が上層の密度にたいして増加していくとき，半円形の山を透過していくレーリー波の透過性は次第に良くなってゆく．実際の地層では，一般に下層へゆくほど媒質の密度は増加して行く．したがってこの実際の地層構造はレーリー波の透過性を助けていることになる．